5-2016

Measurement of Water Ice Accumulation on a First Surface Gold Mirror under Cryogenic, High-Vacuum Conditions

William Hayden Stevens
University of Tennessee - Knoxville, bxv437@vols.utk.edu

To the Graduate Council:

I am submitting herewith a thesis written by William Hayden Stevens entitled "Measurement of Water Ice Accumulation on a First Surface Gold Mirror under Cryogenic, High-Vacuum Conditions." I have examined the final electronic copy of this thesis for form and content and recommend that it be accepted in partial fulfillment of the requirements for the degree of Master of Science, with a major in Mechanical Engineering.

Trevor M. Moeller, Major Professor

We have read this thesis and recommend its acceptance:

L. Montgomery Smith, Joseph A. Wehrmeyer

Accepted for the Council:
Carolyn R. Hodges

Vice Provost and Dean of the Graduate School

(Original signatures are on file with official student records.)

Measurement of Water Ice Accumulation on a First Surface Gold Mirror under Cryogenic, High-Vacuum Conditions

A Thesis Presented for the
Master of Science
Degree
The University of Tennessee, Knoxville

William Hayden Stevens
May 2016

DEDICATION

This thesis is dedicated to my beautiful wife Brianna and my family. Thank you for all of your love and support.

ACKNOWLEDGEMENTS

The Author wishes to acknowledge everyone involved in helping with this thesis. Thank you to my advisor, Dr. Trevor Moeller, for all of your advice, patience, and technical expertise, and for giving me the opportunity to work on such an interesting and unique project. Thanks to Dr. Monty Smith for all of his help and technical expertise. Thanks to Dr. Joseph Wehrmeyer for taking the time to serve on my committee. Thanks to Doug Warnberg for his patience and many hours spent teaching me how to assemble a successful experimental set-up. Thanks to Joel Davenport, Jonathan Kolwyck, Andrew Davis, and Alexander Terekhov for their help in the lab. Thanks to my wife, family, and friends for their encouragement and support. Thanks to the people at Physical Sciences Inc. and AFOSR who supported this work. This work was supported by Physical Sciences Inc. and AFOSR under an STTR. This thesis has been approved for public release under ID number AEDC2016-098.

ABSTRACT

Spacecraft optical components must be tested in vacuum chambers in order to achieve “space-like” conditions on earth. To simulate the low temperatures experienced in space, optical components are often cryogenically cooled in the vacuum chamber. Outgassing of contaminants, such as water molecules, from the metal walls of the vacuum chamber occur under high vacuum conditions. These free water molecules accumulate and freeze on the cryogenic optical surfaces, which affects performance and reflectivity.

A multiple beam interference set-up was used to measure the accumulation of a water ice film on a first surface gold mirror under cryogenic, high vacuum-conditions. Zeolite molecular sieves were used to introduce water vapor into the vacuum chamber. Once inside the chamber, the water molecules were allowed to accumulate and freeze on a cryogenically cooled first surface gold mirror. The external interferometer set-up was used to measure the ice film thickness over time. Simultaneously, a quartz crystal microbalance was used to measure the ice film accumulation. Comparing the thickness results showed that the laser interferometer set-up is an accurate and reliable technique for measuring the water ice film accumulation on the first surface gold mirror.

To advance the current multiple beam interference technique, a new expanded beam interferometer was developed for measuring ice accumulation at multiple locations on the gold mirror. A beam expander was placed on the laser which increased the beam diameter by four times the original size. This expanded beam measured the ice film thickness on a larger portion of the mirror using a custom designed photodiode array. These results were again compared with those obtained from the widely used QCM technique. The comparison showed that the expanded beam interferometer set-up is an accurate and reliable technique for measuring the water ice film accumulation at multiple locations on a first surface gold mirror by agreeing with QCM results to within 2.8%.

TABLE OF CONTENTS

LIST OF TABLES

LIST OF FIGURES

1. INTRODUCTION

1.1 Overview

As humans venture deeper into space, our understanding of the effects on spacecraft components must continue to grow. Modern spacecraft utilize many optical components such as lenses, mirrors, sensors, and solar arrays during missions. These components need to absorb, reflect, or transmit light radiation in order to operate properly. Many times, because the optical components are at cryogenic temperatures, contaminants surrounding the spacecraft will deposit on the optical surfaces and interfere with performance. The main sources of these contaminants are formed by spacecraft combustion products, outgassing of spacecraft materials, and waste removal [1]. It is also known that contaminants, such as water particles in the rings of Saturn, exist naturally in space [2]. Eventually a thin film of cryo-deposit develops on the surface of the optical components. This thin layer becomes detrimental to performance and can result in poor measurements or even cause the instruments to fail.

Similarly, earth-based testing of optical components experiences the same cryo-deposition problem in vacuum chambers. For space simulation on earth, vacuum chambers typically achieve pressures ranging from 10^{-4} – 10^{-11} torr [3]. Most vacuum chambers used for testing are made of metal, such as stainless steel. Metal surfaces are very rough and have microscopic crevices. Figure 1.1 shows a scanning electron microscope image of a 304SS surface [4]. Each time the chamber is exposed to atmosphere, water molecules from the air absorb on the surface which is significantly larger on the microscopic scale due to the small cracks and channels of the metal. As the chamber pumps down, the walls become exposed to high vacuum conditions, and the water molecules are released into the chamber in a process known as outgassing.

Due to this phenomena, a need has become apparent for the detection, monitoring, and mitigation of ice layer accumulation on optical components. The University of Tennessee Space Institute (UTSI) has been working to meet this

need. UTSI was charged with the task of incorporating a multiple beam interference setup for ice film detection and developing a new expanded beam interferometer for monitoring ice accumulation thickness in multiple locations. The vacuum chamber facility at UTSI was used to perform these tests. The small chamber at UTSI was pumped down to high-vacuum conditions, and a cryo-pump was used to bring the interior components down to cryogenic temperatures. Using an effusion cell and zeolite molecular sieves, water molecules were introduced into the vacuum chamber with the intention of accumulating an ice layer on a first surface gold mirror.

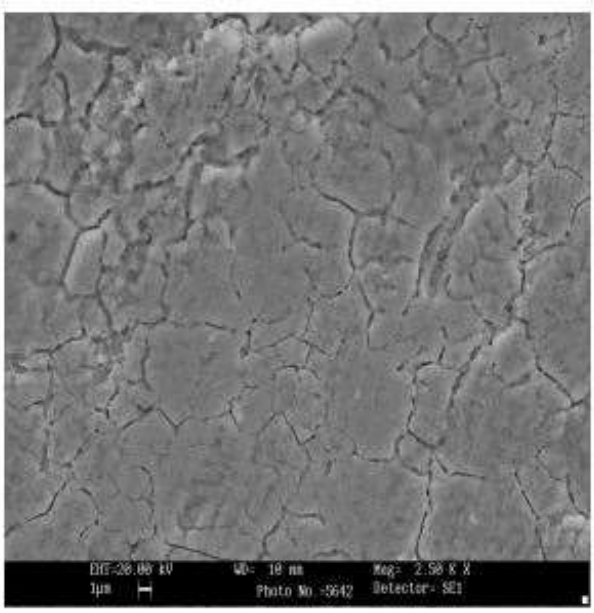

Figure 1.1: SEM image of 304 stainless steel [4].

An unexpanded beam interferometer set-up was used to detect and monitor the ice layer thickness at one location on the mirror. This technique, which has been used in the past for making thin film measurements [8], uses the multiple-beam interference that results from light reflected off a mirror with a thin film on the surface. The thickness results from the optical interferometer data were compared with thickness measurements from a quartz crystal microbalance (QCM) in the

chamber, which is commonly used for validation in thin film measurements. The comparisons proved that the interferometer monitoring device is an accurate and reliable technique for making ice film measurements in a single location. Next, an expanded beam interferometer set-up was developed and used for making ice thickness measurements at multiple locations on the mirror surface. The expanded beam covered a larger surface area of the mirror and utilized an array of photodiodes for measuring data. This new technique provided an understanding of how the ice layer was accumulating on different locations of the mirror. Thickness results from the expanded beam interferometer data were again compared to the QCM results.

1.2 Background

Before describing the experimental set-up, it is important to discuss the background of measuring water ice films. First, the behavior of water ice under low pressure and temperature conditions must be understood. Next, in order to grow a relatively thick ice film, an effective way of introducing additional water molecules into the vacuum chamber must be developed. Finally, frost formation on cold surfaces and techniques for measuring thin film thickness are discussed.

1.2.1 Previous Work

Three forms of ice are prevalent in cryogenic vacuum environments. These are cubic ice, I_c, low density amorphous, LDA, and high density amorphous, HDA, ice. It is still unknown as to how exactly the ice transitions between these phases, but typically it follows according to Table 1.1 [3]. For this experiment, the temperature of the optical components was approximately 50-60 K. Therefore, the LDA density was used for these calculations and is given by the CRC Handbook of Chemistry and Physics as 0.934 g/cm^3 [5].

Table 1.1: Ice formations in cryo-vacuum [3].

Form	Density (g/cm^3)	Temperature Range (K)
I_h (hexagonal)	0.92	> 160
I_c	0.93	136 – 160
LDA	0.94	15 – 136
HDA	1.17	< 15

Several experiments were conducted in order to determine the most efficient way of introducing water molecules into the vacuum chamber. After testing calcium sulfate dehydrate, cobalt (II) chloride hexahydrate, and zeolite molecular sieves, it was determined that the zeolite sieves introduced an appropriate amount of water while leaving very little leftover residue in the chamber. The type of zeolite used for this experiment was the Linde A-type zeolite with the 3Å pore opening. This type was used because it only absorbs NH_3, H_2O, and some H_2. Other zeolite sizes such as the 4Å type absorb H_2O, CO_2, SO_2, H_2S, C_2H_6, C_3H_6, and ethanol [6].

1.2.2 Frost Formation on Cold Surfaces

Frost formation on a cold surface with a large temperature gradient between the cold surface and the gas is a very complex process. In this experiment, the water vapor was at room temperature, and the cold optical surface reached a temperature of approximately 45 K. When the room-temperature gas reaches the cold surface, some particles deposit on the surface while others flow past and sublime. Initially the deposit forms a few micro-sized “patches” of frost which act as traps for additional water particles. It can be assumed that the temperature of the frost “patches” are approximately equal to the temperature of the cold surface. However as the clumps of frost accumulate and grow, a thin layer of frost forms and covers the cold surface. This layer has an insulating effect and results in an increase in the frost surface temperature [7]. As the frost continues to accumulate, stresses form within the ice layer. This stress can ultimately lead to fracturing of

the ice film. The little known information about fracturing of LDA water films is that there is a critical thickness for fracture that depends significantly on the film temperature [3].

1.2.3 QCM Thickness Monitoring

A quartz crystal microbalance (or QCM) measures the mass deposition rate per unit area (g cm^{-2} s^{-1}). A voltage is applied to the quartz crystal which causes it to oscillate at its resonant frequency, and the resulting voltage is input to a frequency counter. The QCM used for this experiment was the Inficon QPod with a 6 MHz resonant frequency. As the thin film mass builds on the quartz crystal surface, the resonant frequency of the crystal decreases. With this knowledge, a film thickness can be determined [8]. The fundamental mode of vibration in a quartz crystal is given as:

$$f_o = \frac{\sqrt{\mu_q/\rho_q}}{2t}, \quad (1)$$

where μ_q, ρ_q, and t are the shear modulus of quartz, the density of quartz, and the crystal thickness. The frequency shift resulting from film deposition is given by Sauerbrey [9] as

$$\Delta f = -\left(\frac{2f_o^2}{\sqrt{\mu_q \rho_q}}\right)\left(\frac{\Delta m}{A}\right), \quad (2)$$

where Δm is the change in the total (crystal and film) mass and A is the crystal active collection area. A film thickness can be determined from the change in crystal mass using equation (3) [10].

$$x = \frac{m}{A\rho}, \quad (3)$$

In equation (3), x is the film thickness, m is the total mass deposited from equation (2), A is the crystal area, and ρ is the film density. Equation (2) is only valid if the film thickness is small compared to the crystal thickness. Therefore, an improved method for determining the deposited film mass, known as the Z-match technique, is given in equation (4) and is valid for a frequency decrease of up to 40% of the unloaded frequency [8]. The mass per unit area (g/cm^2) on the crystal is given as

$$\left(\frac{m}{A}\right)_f = \frac{N_q \rho_q}{\pi f_c Z} \tan^{-1}\left[Z \tan\left(\frac{(f_q - f_c)}{f_q}\right)\right] (1x10^{-8}), \quad (4)$$

where N_q is a frequency constant of the cut quartz, ρ_q is the density of the quartz, and f_q and f_c are the frequencies of the clean gold coated quartz crystal and the measured frequency, respectively, when the crystal is covered with a layer of ice [8]. The Z term given in equation (4) can be calculated by

$$Z = \left(\frac{\rho_q G_q}{\rho_f G_f}\right)^{1/2}, \quad (5)$$

where ρ_f is the density of the ice and G_q and G_f are the shear moduli of quartz and ice, respectively [11]. The ice film thickness measured by the QCM from the above equations can be used as a comparison for other techniques measuring film thickness such as multiple beam interference.

1.2.4 Theory of Light Interactions with Cryodeposits

In order to develop a film thickness monitor, it is important to discuss the underlying subject of light interactions with cryodeposits. When emitted light is incident on a thin film, there are components of the light that are absorbed, reflected, or transmitted by the film. In this experiment, only the case of reflection and transmission was considered. Figure 1.2 shows a schematic of the light scattering model [12]. This model considers all possible constructive interference

between reflecting rays and is the most general. The following assumptions were made for the derivations:

- The incident light is perfectly collimated and monochromatic.
- The substrate (gold) is a perfect specular reflector.
- Cryodeposits reflect and refract light according to Snell's Law.
- A 180° phase shift occurs when light traveling through one medium is reflected by another which has a higher refractive index.
- There is no gap, cavity, or contamination between the cryodeposit and substrate surface.

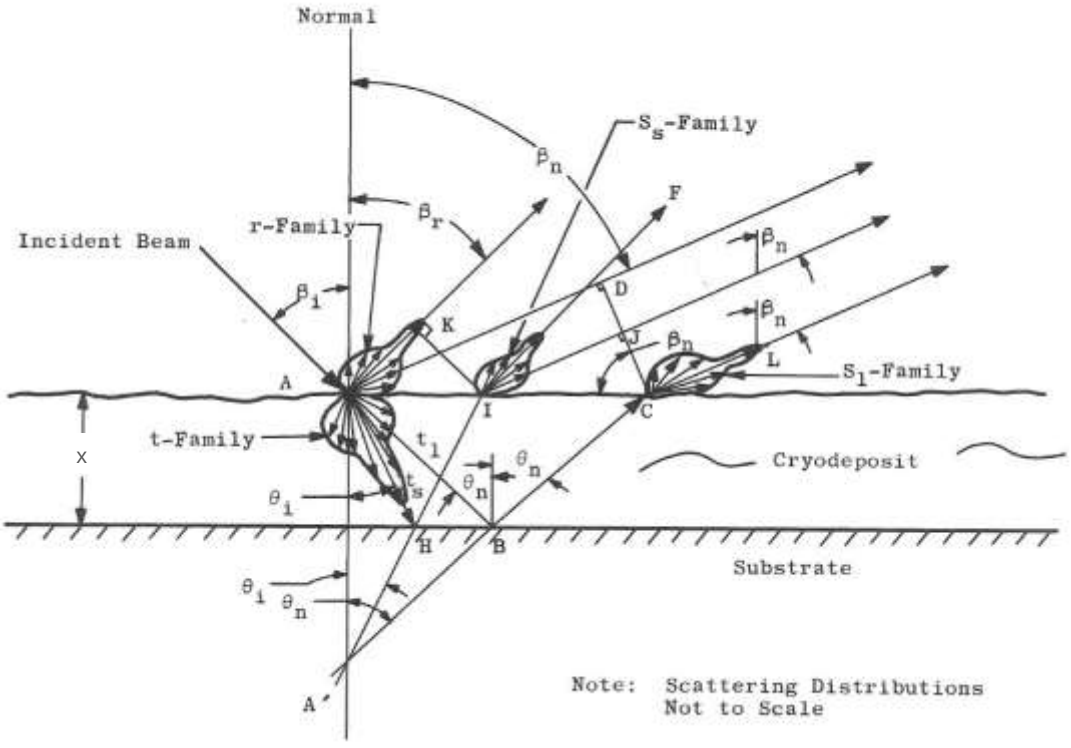

Figure 1.2: Schematic of light scattering model [12].

Using the optical path difference between adjacent rays and the assumptions listed, the following equations were derived for the model [12].

$$x = \frac{m\lambda}{2\mu\sqrt{1-\frac{\sin^2(\beta_n)}{\mu^2}}}, \tag{6}$$

$$x = \frac{n\lambda}{2\mu\left(\frac{1}{\sqrt{1-\frac{\sin^2(\beta_i)}{\mu^2}}} - \frac{\sin(\beta_i)\sin(\beta_n)}{\mu^2\sqrt{1-\frac{\sin^2(\beta_i)}{\mu^2}}} - \sqrt{1-\frac{\sin^2(\beta_n)}{\mu^2}}\right)}, \tag{7}$$

In equations (6) and (7), *x* is the cryodeposit thickness, m and n are integer differences in the optical path lengths, λ is the wavelength of incoming light, μ is the refractive index of the cryodeposit, β_n is the angle to the normal of an arbitrary ray CL (see Figure 1.2), and β_i is the incident angle of incoming light. The two different equations are for two different cases of constructive interference. Equation (6) is derived for constructive interference between the specularly reflected, retransmitted, and refracted component of an arbitrary scattered transmitted ray in the t-family and a reflected and scattered ray in the r-family which has the same angle to the normal, β_n. Equation (7) is derived for constructive interference between the refracted component of the S_1-family caused by an arbitrary t-family ray and a scattered ray in the S_s-family caused by t_s, which has the same angle to the normal. The two equations are given because of the uncertainty as to which type of constructive interference dominates [12].

1.2.5 Multiple Beam Interference for Experiment

For the thin film calculations in this experiment, the assumption was made that only the refracted and specularly reflected components of the rays within the thin film compared to the specularly reflected incident ray made the greatest contribution to the interference. Figure 1.3 describes this simplified model [13].

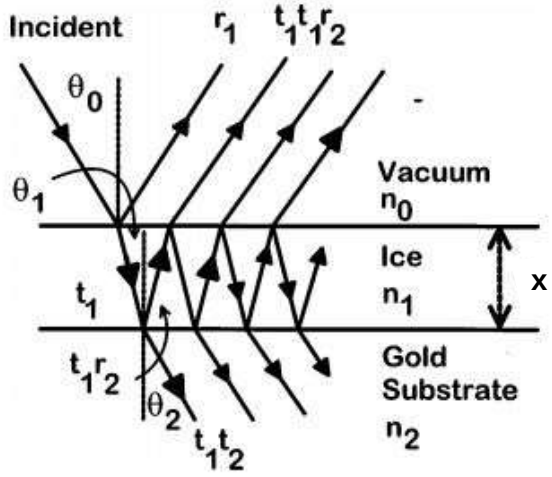

Figure 1.3: Reflection from a thin film on a gold substrate [13].

The difference in optical path lengths of the reflected and transmitted fronts is given by Hecht and Zajac [14] as

$$\Delta OPL = 2n_2 x cos\theta_2, \tag{8}$$

where n_2 (n_1 in Figure 1.3), x, and θ_2 (θ_1 in Figure 1.3), are the refractive index of the ice film, thickness of the ice film, and the angle of propagation of the light in the thin film as found by Snell's Law. The phase shift occurring in adjacent reflected and transmitted wave fronts is given as

$$\delta = \frac{2\pi}{\lambda}\Delta OPL = \frac{4\pi n_2 x cos\theta_2}{\lambda}, \tag{9}$$

where δ is the phase shift between reflected and transmitted wave fronts and λ is the wavelength of incoming light [14]. Summing the infinite number of reflected rays yields the total magnitude. Squaring the magnitude results in the intensity reflectance ratio given by

$$R = \left|\frac{r_{12}+r_{23}e^{-i\delta}}{1+r_{12}r_{23}e^{-i\delta}}\right|^2, \tag{10}$$

where the thickness x can be found in the parameter δ as shown in equation (9). Parameters r_{12} and r_{23} represent the complex reflection coefficients for light interaction at the boundaries between the vacuum (medium 1) and cryodeposit (medium 2) and the cryodeposit and optical component coating (medium 3) [8]. The components r_{12} and r_{23}, using slightly different notation, are given for light polarized such that its electric field is perpendicular to the plane of incidence by the Fresnel Equation as

$$r_{12} = \frac{n_1 \cos\theta_1 - n_2 \cos\theta_2}{n_1 \cos\theta_1 + n_2 \cos\theta_2}, \tag{11}$$

$$r_{23} = \frac{n_2 \cos\theta_2 - n_3 \cos\theta_3}{n_2 \cos\theta_2 + n_3 \cos\theta_3}, \tag{12}$$

where n_1, n_2, n_3, and θ_1 (θ_0 in Figure 1.3) are the refractive indices of vacuum, ice, and gold and the angle of incidence of incoming light. Angles θ_2 and θ_3 (θ_1 and θ_2 in Figure 1.3) are the angles of propagation of the light in the film and substrate material and can be found by using Snell's Law [13, 15].

For this experiment, a 50mW diode laser with wavelength 450 nm was used. The shorter wavelength was used because it provides better thickness resolution, which is recommended when cryodeposit layers are thin [12], and it also provides greater visibility in the reflectance when a gold substrate is used. Therefore with λ=450nm, the refractive indices of vacuum, ice, and gold are given as $n_1 = 1$, $n_2 = 1.3157$ [16], and $n_3 = 1.502 + 1.8785i$ [17]. A more detailed explanation of determining the refractive index of condensed gases at different wavelengths is given by Wood and Smith [18].

1.2.6 Interferometer Thickness Monitoring

The phase shift experienced by the light traversing one pass through the thin film with thickness *x* as a function of time is given by Smith [19] as

$$\delta(t) = \frac{4\pi n_2 cos\theta_2 x(t)}{\lambda}, \quad (13)$$

where *n2*, *θ2*, and *λ* are the refractive index of the water ice film, the angle of light propagation in the film, and the wavelength of incoming light. Due to the oscillatory behavior of the multiple beam interference, the reflected intensity fluctuates between a maximum and a minimum value. Therefore, the corresponding change in film thickness over each period of modulation is

$$\Delta x = \frac{\lambda}{2n_2 cos\theta_2}, \quad (14)$$

In the thickness monitoring program given by Smith [19], the growth rate is assumed to remain constant over each modulation cycle and theoretical reflectance intensity ratios are calculated based on λ = 450nm and different time intervals 0 < t < T for one cycle.

$$x_T(t) = \frac{\lambda t}{2T n_2 \cos\theta_2}, \quad (15)$$

Normalized cross-correlation coefficients are computed using the theoretical data and the experimental intensity reflectance data for time periods differing by one sample period. The optimal value from the cross-correlation technique gives the thickness increase over the measured time period. Therefore, ice thickness values can be computed at discrete times resulting in the total ice film accumulation from beginning to end of an experiment [19].

2. EXPERIMENTAL SETUP AND INSTRUMENTATION

The following section describes the setup of the “20V” vacuum chamber in the UTSI Vacuum Chamber Facility and the instrumentation used during the experiments.

2.1 Main Chamber Overview

The vacuum chamber used at the UTSI Vacuum Chamber Facility is a 0.6 meter diameter, 0.45 meter tall stainless steel chamber. It is fitted with a roughing pump, turbo-pump, and cryo-pump. There are 6 available ports for use spread equally around the chamber. Two of the ports are used for the laser interferometer. One of the large ports was used to connect the water introduction apparatus as shown in Figure 2.1. The pressure is monitored using two Kurt J. Lesker® Company convection vacuum gauges (275 Series) and one digital ion gauge (KJLC 354 Series).

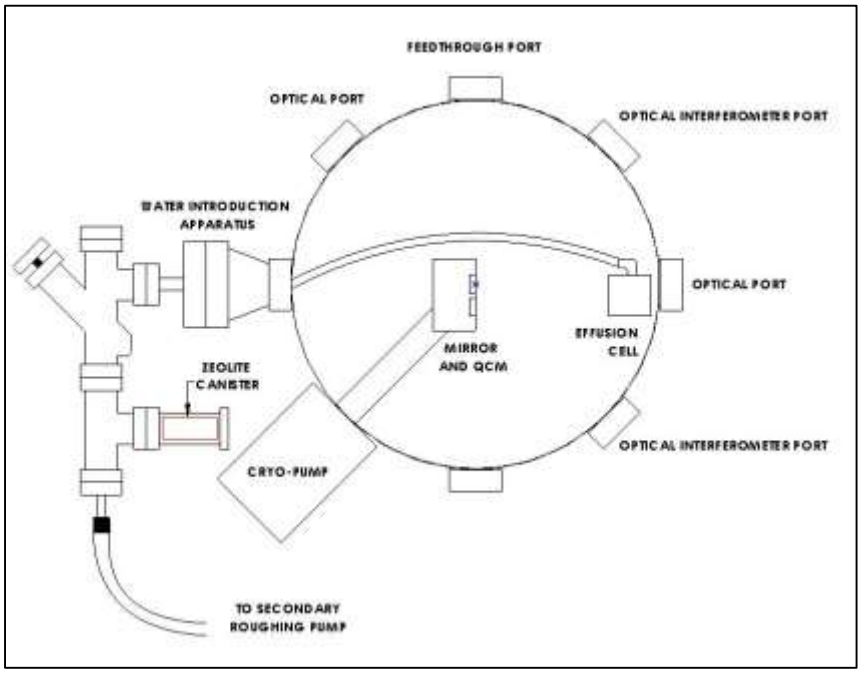

Figure 2.1: Top view of “20V” chamber.

Once the chamber was closed, the roughing pump removed the bulk of the atmospheric air in the chamber. When the pressure reached a minimum at approximately 10^{-3} torr, the turbo-pump was turned on. The turbo pump would bring the chamber pressure down to approximately 10^{-6} torr. Since the number of air particles remaining in the chamber was very small relative to the main chamber volume, the cryo-pump was used. The cryo-pump froze many of the remaining molecules that contacted its surface and allowed the pressure to drop to approximately 10^{-9} torr. This entire process would take about 1 day. Figure 2.2 shows the previously described vacuum chamber at UTSI.

The water introduction apparatus was closed off from the main test chamber. A secondary roughing pump was connected to this section in order to control the pressure separately from the main chamber and was capable of pumping the zeolite section down to approximately 10^{-2} torr. This setup allowed for easy access and removal of zeolite samples during a test run.

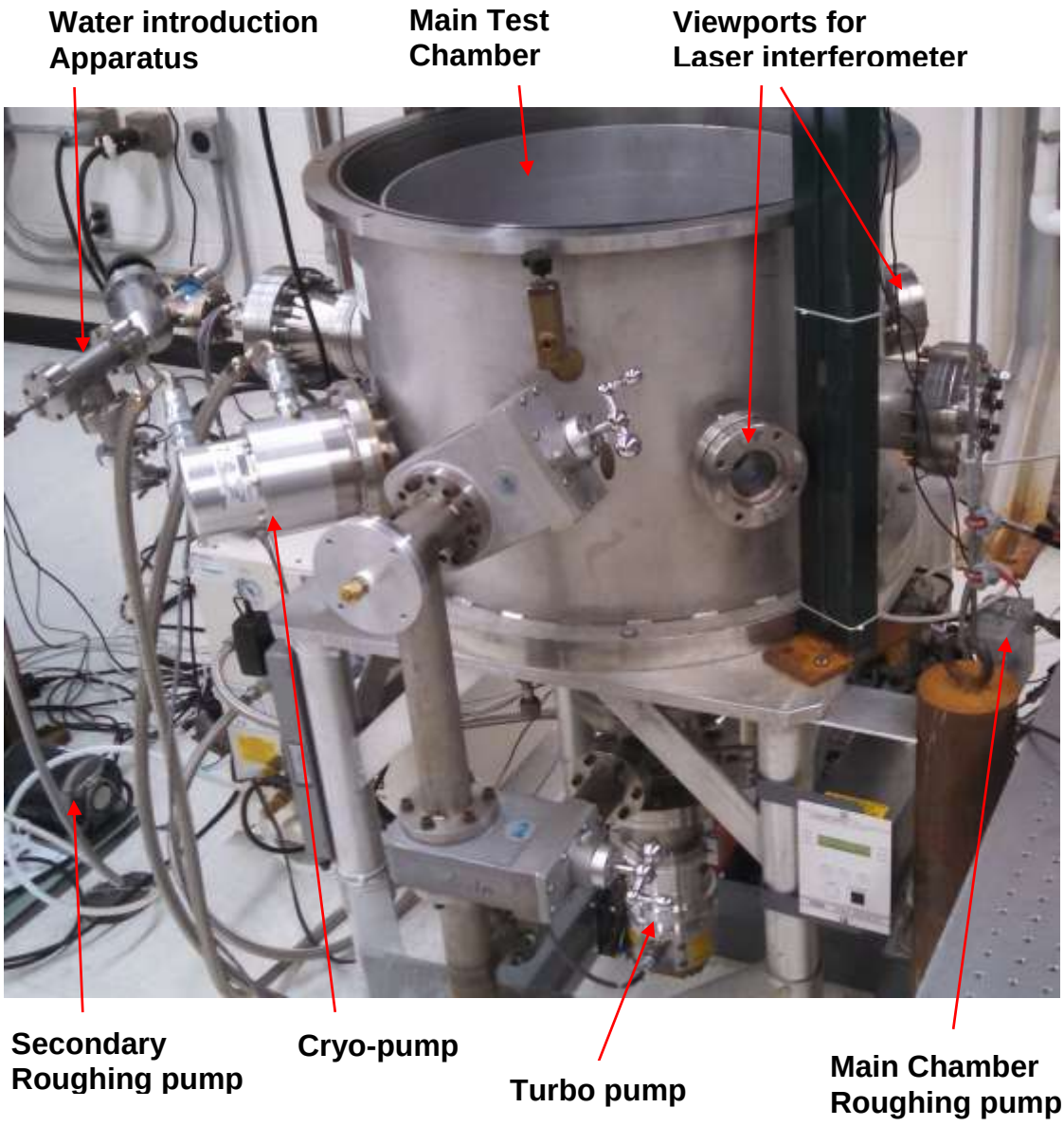

Figure 2.2: UTSI vacuum chamber.

2.2 Water Introduction Apparatus

Zeolite molecular sieves were used to introduce water into the chamber. The method of introducing water into a vacuum chamber was studied extensively by Rogers [6]. The same water introduction apparatus was used in this experiment. Figure 2.3 below shows the setup.

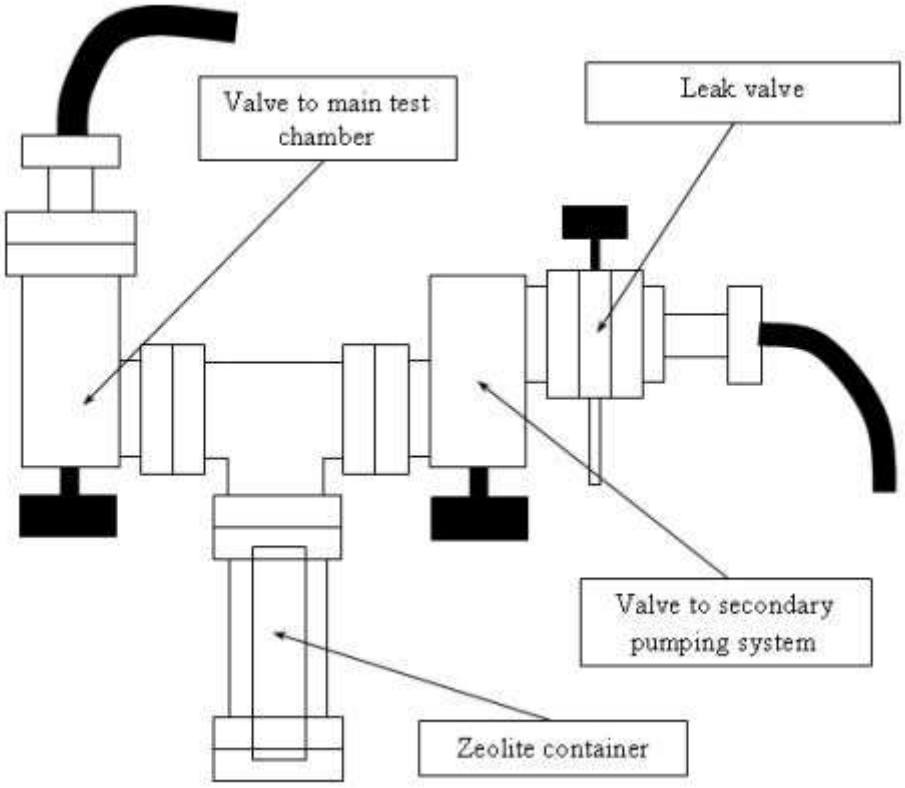

Figure 2.3: Schematic of water introduction apparatus [6].

The zeolite sieves were vacuum baked in order to drive off and remove contaminants. Approximately 14g of zeolite was hydrated with 2mL of de-ionized water. Once hydrated, the sieves were placed inside the introduction apparatus. The zeolite section was closed off from the rest of the chamber using the main test chamber valve shown in Figure 2.3. Once the main chamber had reached high vacuum conditions (10^{-9} torr), the zeolite section was pumped down using a roughing pump. Once the pressure in the zeolite section bottomed out (10^{-2} torr),

the main test chamber valve was opened. Due to the pressure gradient between the main chamber and the zeolite section, a flow of water molecules was introduced into the chamber. At the end of the experiment, the dried out zeolite was replaced with freshly hydrated zeolite for the next run. Figure 2.4 below shows the water introduction apparatus used in the experiment.

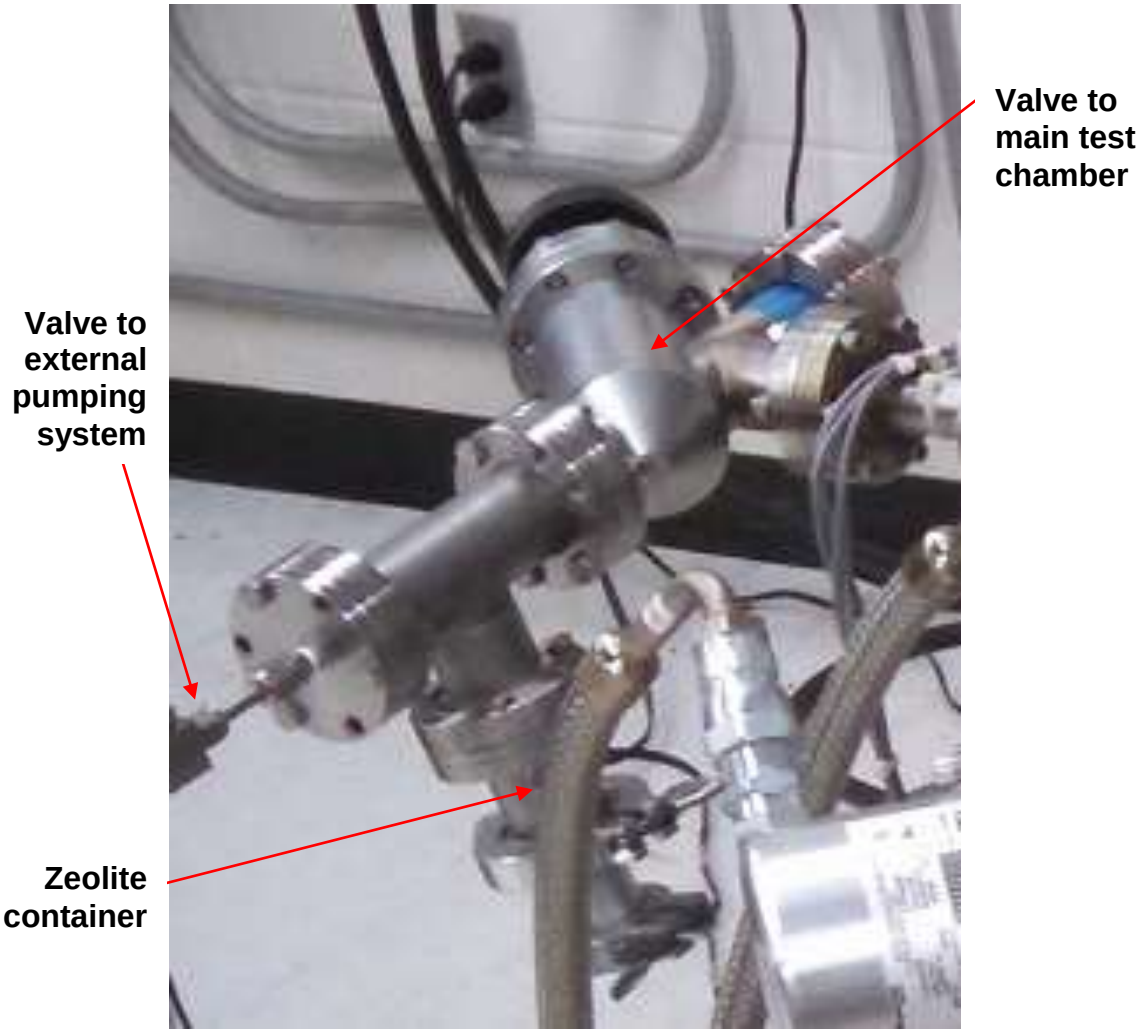

Figure 2.4: Water introduction apparatus.

2.2.1 Effusion Cell

The purpose of the effusion cell for this experiment was to introduce a consistent distribution of water molecules into the chamber and incident on the gold mirror and QCM. The effusion cell used was designed using parameters and specifications from a previous effusion cell used by Labello [3] and Rogers [6], which is shown below in Figure 2.5 [3].

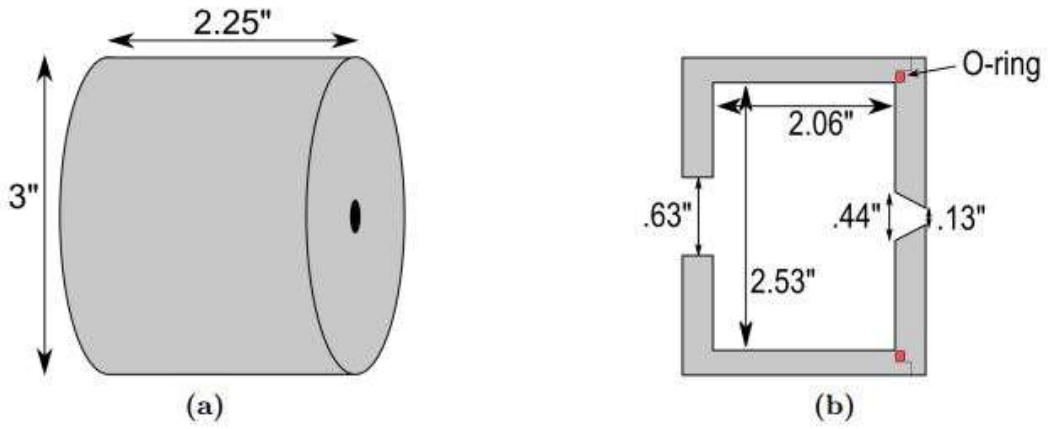

Figure 2.5: (a) External dimensions and (b) cutaway view of the effusion cell previously used [3].

The effusion cell was designed to produce a cosine distribution of water vapor under free molecular flow [3]. This design was crucial in properly directing the water vapor towards the mirror and QCM surfaces and growing a uniform ice film. The effusion cell model for this experiment incorporated the same dimensions and can be seen in Figure 2.6. The effusion cell legs were mounted on an axis of rotation in order to allow for precision adjustments. It was placed on the floor of the vacuum chamber and angled at 32 degrees from the mirror surface as seen in Figure 2.7. At this angle, the center of the cosine distribution is centered between the gold mirror and the QCM.

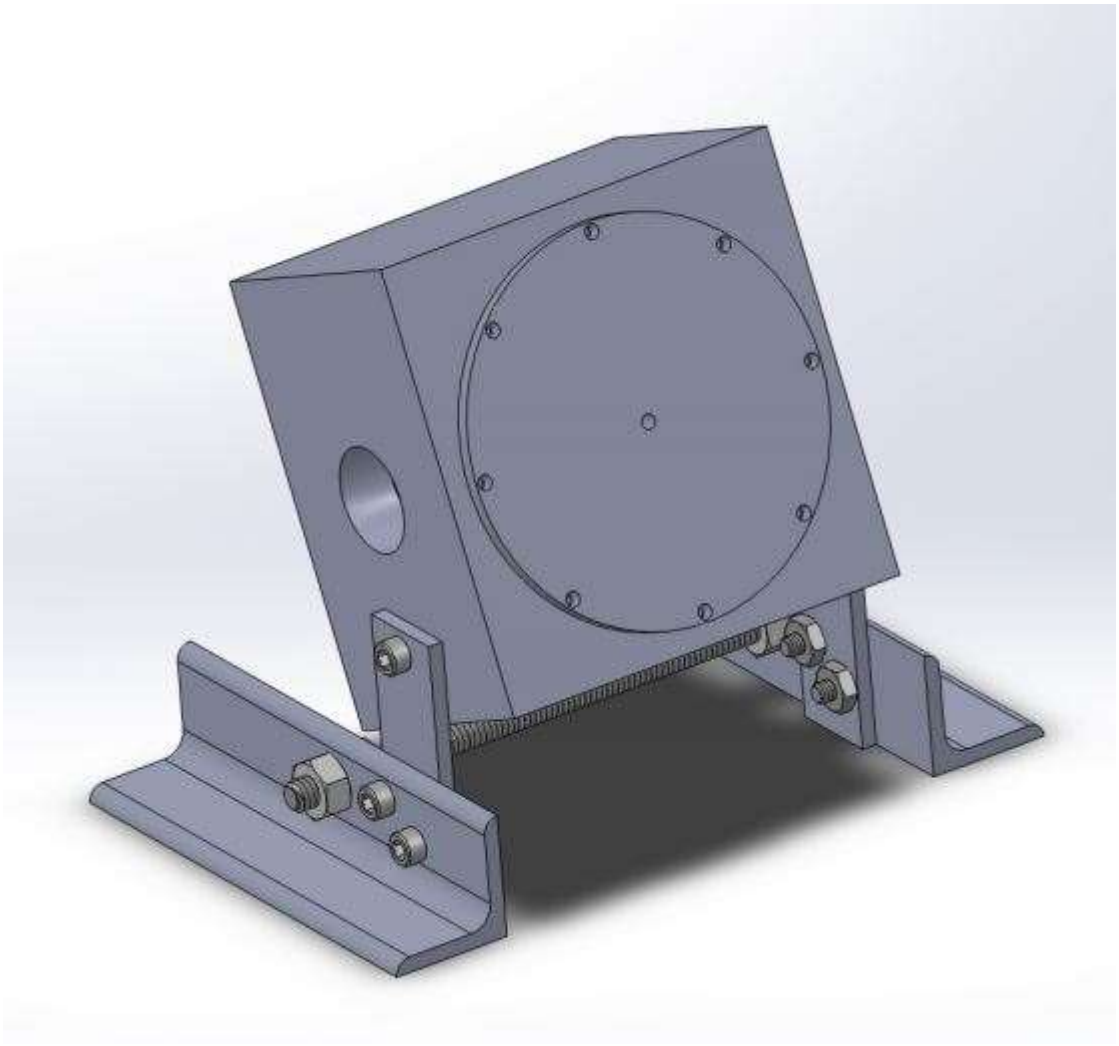

Figure 2.6: SolidWorks model of new effusion cell.

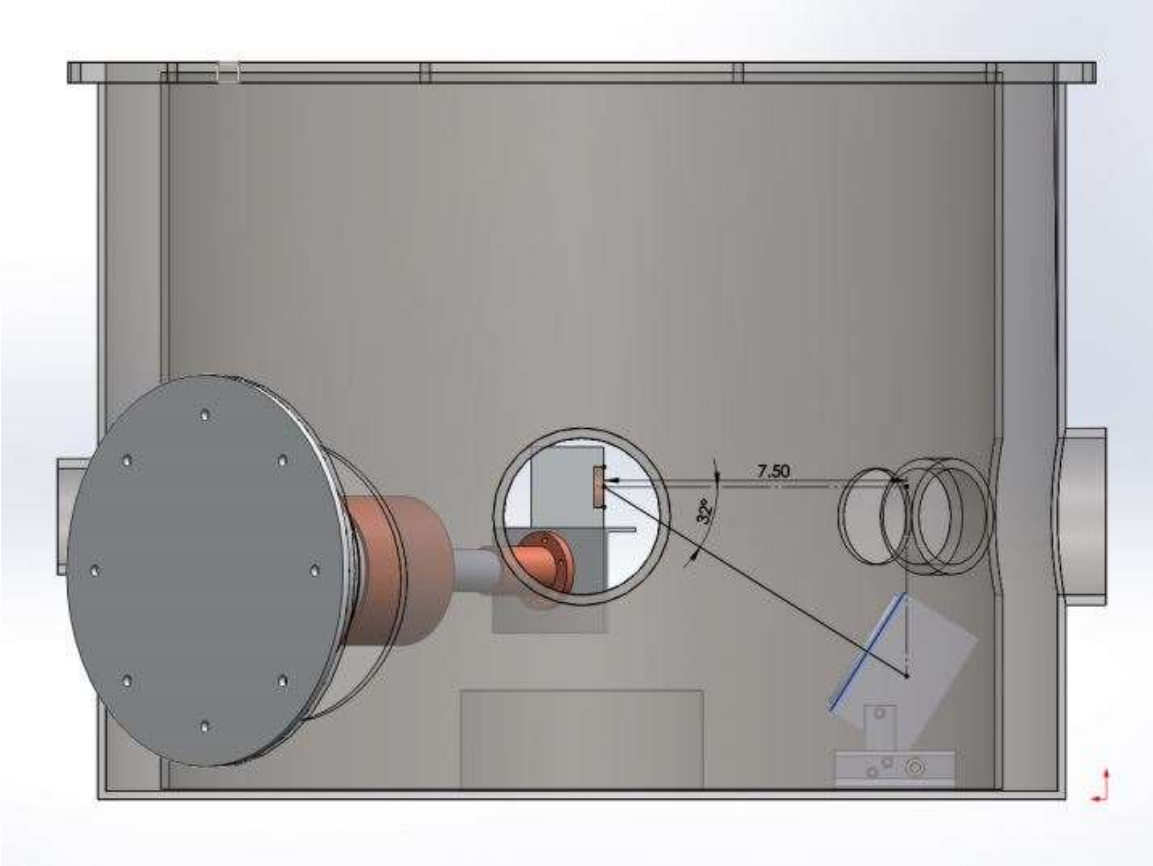

Figure 2.7: Placement of effusion cell inside vacuum chamber.

2.3 Interior Chamber Setup

The critical interior components of the experiment consisted of the cryo-pump mounting stage, or “cold finger”, the mounting bracket, the Thorlabs® precision kinematic mirror mount, a 25.4mm diameter protected gold mirror, a QCM, two cryogenic linear temperature sensors (CLTS), a radiation shield which acted to block incoming radiation from the chamber walls, and the effusion cell. A cryo-liner filled with LN_2 was used in early tests, but was found to have little effect on the mirror and QCM temperatures. The cryo-pump used is a Sumitomo® CH-210 Cold Head. Compressed helium is used to absorb the heat from the environment. The helium cycles through two stages in the pump. Figure 2.8 shows the internal diagram of the Cold Head [20].

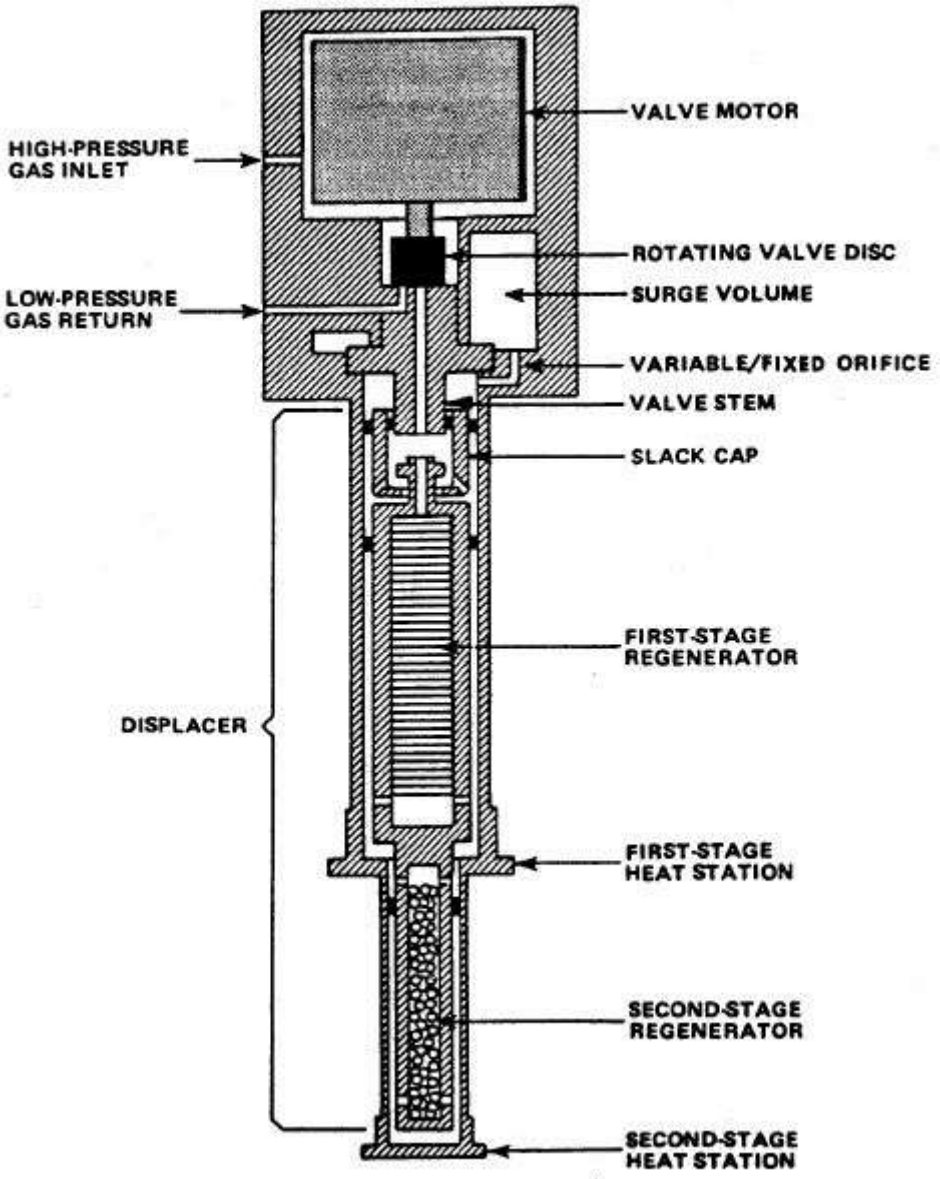

Figure 2.8: Simplified cold head diagram [20].

During the intake stroke, compressed helium is introduced into the first and second stages. As the helium absorbs energy (heat) from the surroundings, its pressure drops. The high temperature helium is then removed during the exhaust stroke. The first stage is capable of reaching 77K, and the second stage can reach 20K [20]. An aluminum bracket was mounted to the second stage of the cryo-pump, and the mirror mount and QCM rested on the aluminum bracket. A cryogenic linear temperature sensor (CLTS) was attached to both the mirror mount and QCM in order to monitor the temperature during the experiment. Finally a copper shield was placed around the second stage of the cryo-pump in order to absorb the radiation coming from the vacuum chamber walls.

The water was forced from the zeolite introduction apparatus (Figure 2.4) into the effusion cell by a pressure gradient. This gradient was due to the high vacuum conditions of the main test chamber and the low vacuum conditions of the zeolite introduction section, which was producing water molecules. A Teflon tube was used in connecting the zeolite apparatus to the effusion cell due to its relatively low outgassing properties under high vacuum. Flexible tubing was necessary for this application because the effusion cell was positioned at the bottom of the chamber. Figure 2.9 shows the interior chamber setup as previously described.

Figure 2.9: Interior chamber components.

2.4 Exterior Chamber Setup

The exterior chamber setup consisted of a laser, beam polarizer, beam splitter, focusing lens, and several photodiodes. The interferometer setup measured the phase shift change of the incident light as it passed through the thin film of ice. This change results in an intensity fluctuation of the incident laser beam. When an intensity ratio of reference light to reflected light was taken, it was possible to determine a film thickness as described in Sections 1.2.5 and 1.2.6. A 450 nm, 50 mW blue laser was used as the light source. The laser passed through a polarizer, which resulted in light with its electric field perpendicular to the plane of incidence, and a beam splitter. The first beam, known as the reference beam, measured the overall laser output with a photodiode. The second beam passed through the chamber window and reflected off the gold surface mirror. This reflected beam was measured by a second photodiode outside the chamber. Figures 2.10 and 2.11 show the experimental setup and optical layout.

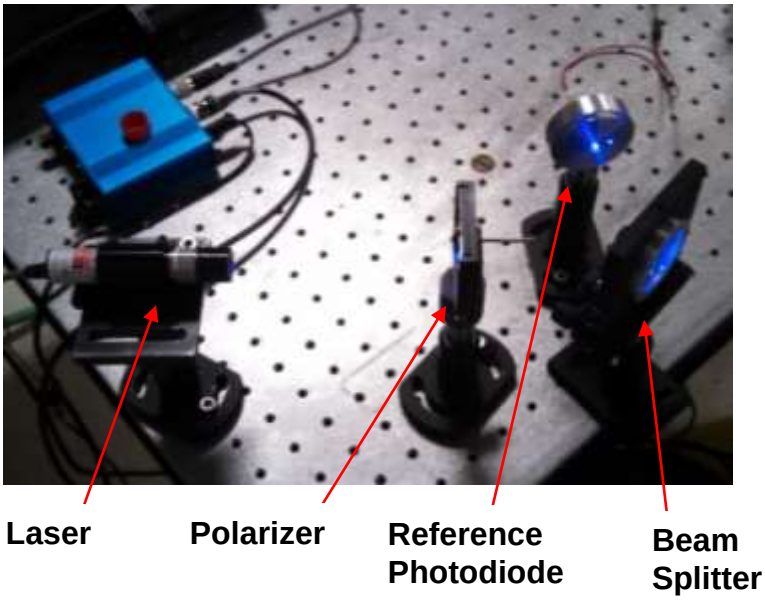

Figure 2.10: Unexpanded beam experimental setup.

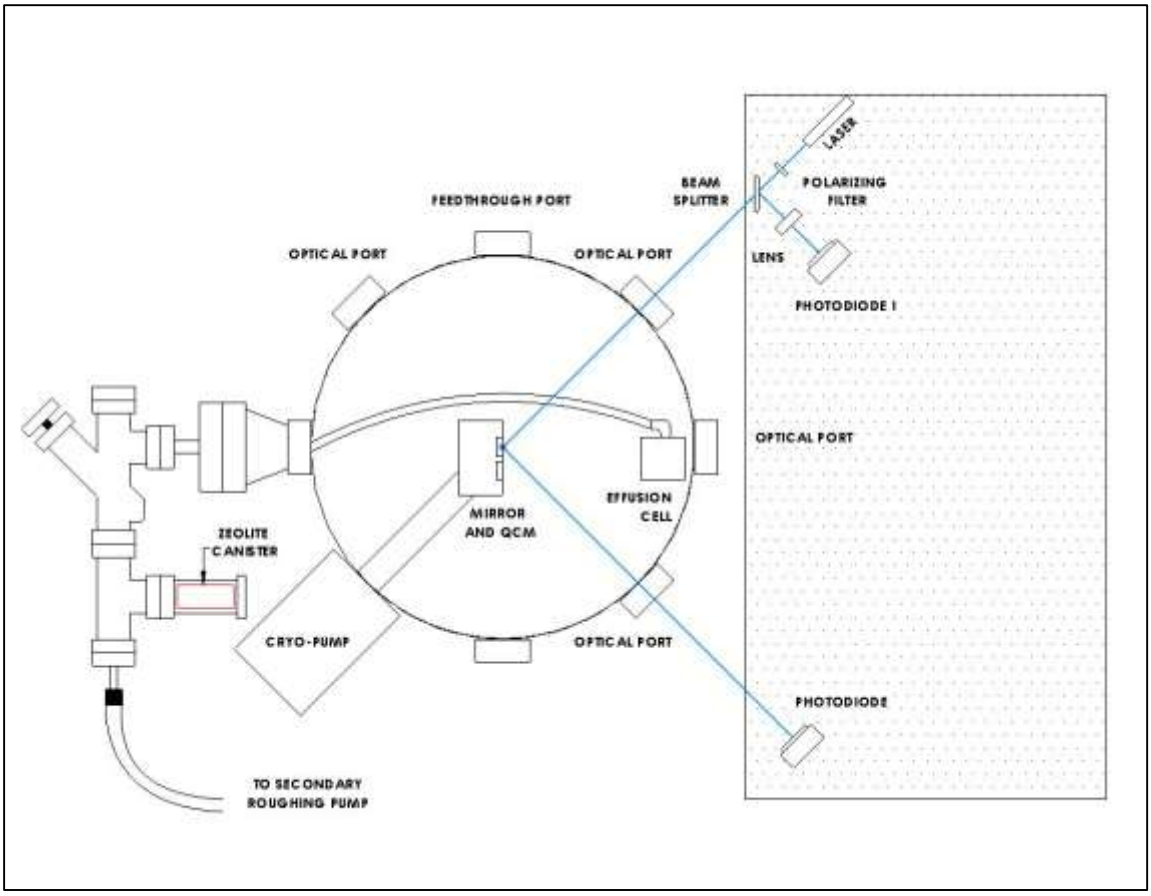

Figure 2.11: Optical schematic (unexpanded beam).

2.4.1 Expanded Beam Interferometer

After several runs with the single point beam interferometer, a new expanded beam interferometer setup was used. The purpose of the expanded beam was to simultaneously measure the ice film thickness at different locations on the mirror. The original laser beam was an elliptical dot beam covering a surface area of approximately 1.5 mm^2. With the 4X beam expander attached, the new beam surface area was approximately 24 mm^2. Pairing this expanded beam with an array of photodiodes allowed for ice film thickness measurements to be made in multiple locations simultaneously during an experimental run. Figures 2.12 and 2.13 show the expanded beam experimental setup and optical schematic. The photodiode array is shown in Figure 2.14 with five photodiodes, however, due to the beam geometry, only three photodiodes were used (PD2, PD3, PD4).

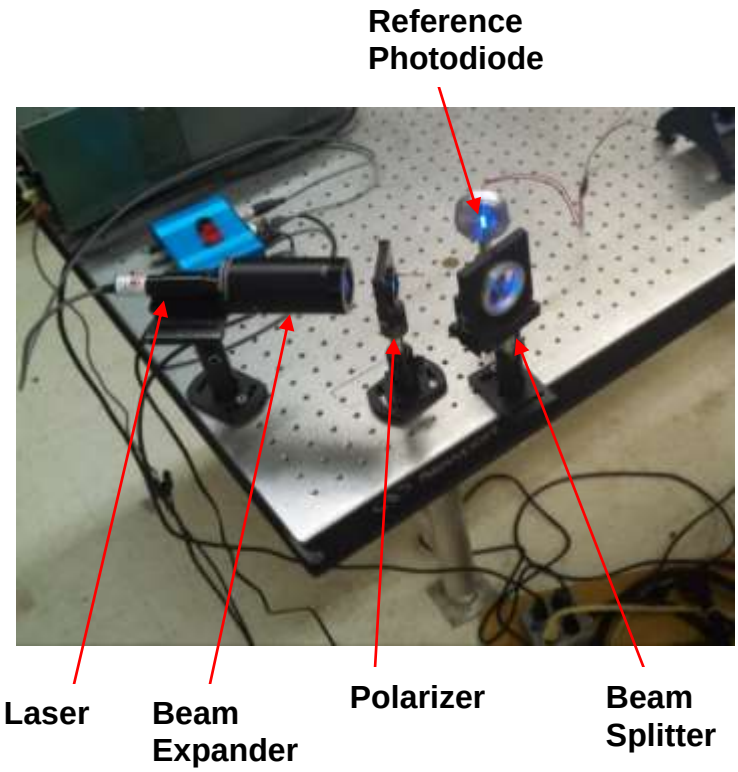

Figure 2.12: Expanded beam experimental setup.

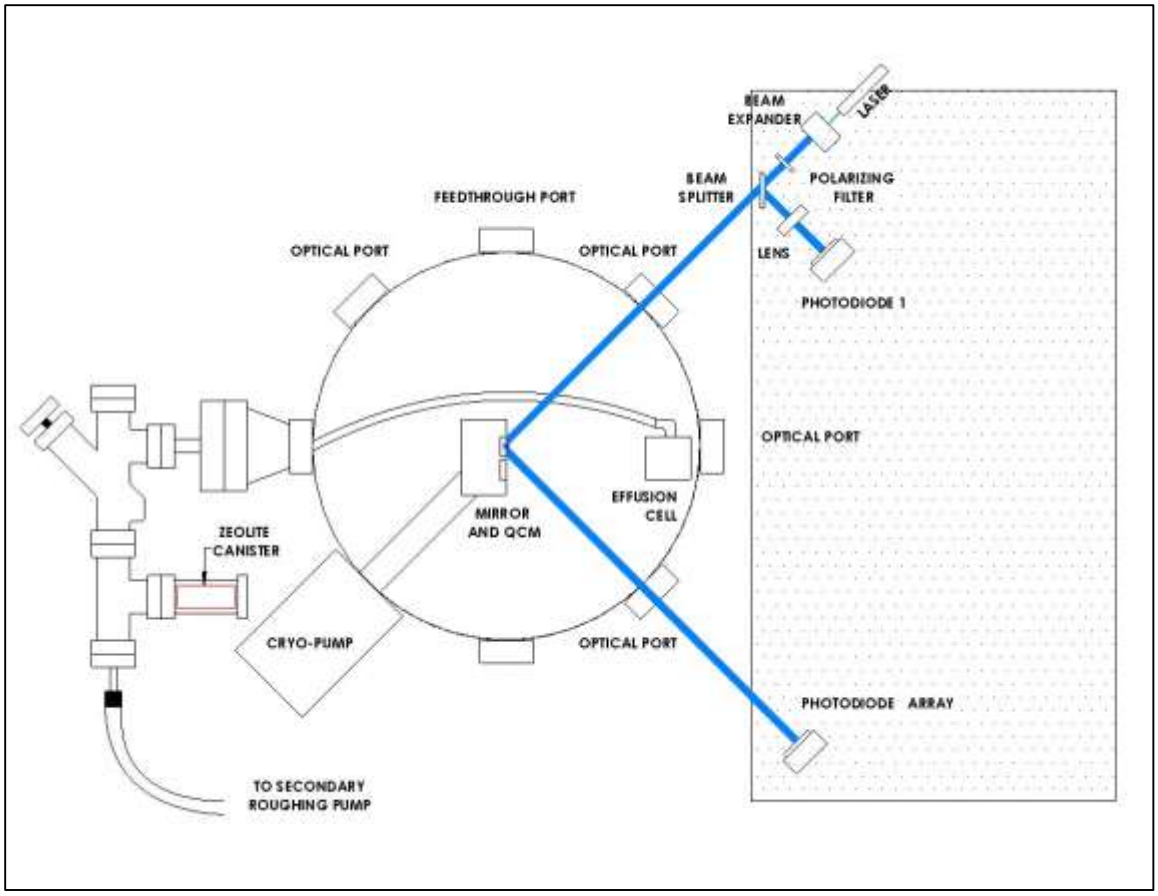

Figure 2.13: Optical schematic (expanded beam).

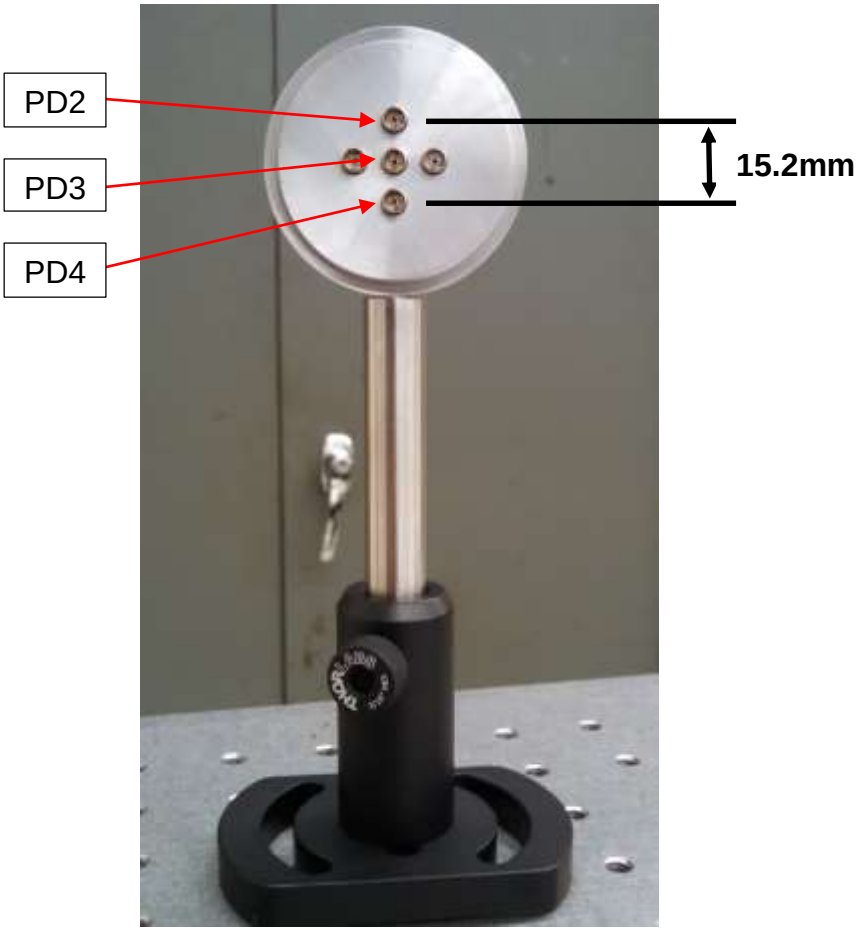

Figure 2.13: Photodiode array.

3. RESULTS

3.1 Basic Pump Down

At the beginning of an experimental run, the mirror, QCM, and effusion cell were aligned in an effort to produce a uniform layer of ice film buildup. Once the interior components were properly aligned, the main chamber was sealed and started pumping down. After about 1 day, with a combination of roughing pump, turbo pump, and cryo pump, the main chamber reached a pressure of approximately 10^{-9} torr. The zeolite section was closed off from the main chamber and pumped separately. Figure 3.1 shows the main chamber pressure during one of the pump down processes before the water molecules were introduced.

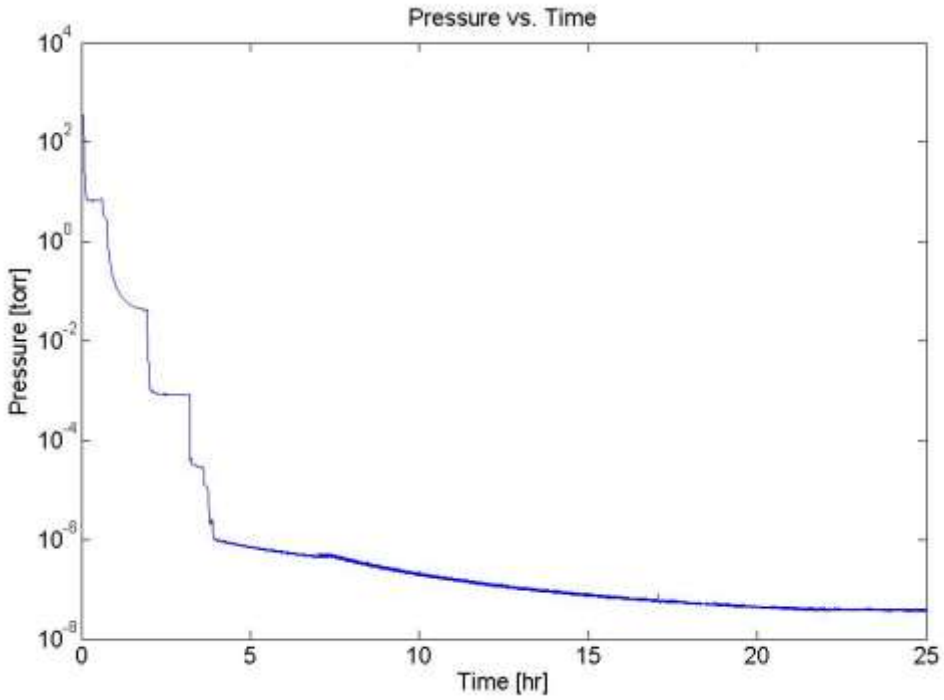

Figure 3.1: Main chamber pressure during one pump down process.

The pressure gauges used in this experiment were a combination of two convection vacuum gauges (one for the main chamber and the other for the zeolite canister) and one digital ion vacuum gauge. The convection vacuum gauges have a cutoff pressure of approximately 10^{-3} torr below which the pressure readings no longer are accurate. The digital ion gauge has an operational pressure range of approximately $10^{-3} – 10^{-9}$ torr. Figure 3.1 shows the pressure bottoming out around 2.5 hours and then a steep drop at 3 hours. The switch between pressure gauge readings was the cause of this. The main chamber pressure reached a minimum value of approximately 10^{-6} torr after 4 hours of pumping. The cryo pump was then turned on which allowed the pressure to continue dropping and begin approaching 10^{-8} torr. Several small plateaus can be seen between the 10^{-2} and 10^{-8} range and are a result of virtual leaks in the chamber.

The temperature of the second stage of the cryo pump was also monitored during one of the pump-down processes. It was important for the cryo pump to obtain temperatures below 70 K in order for the nitrogen gas in the air to condense and freeze, thus dropping the chamber pressure. The plot of temperature of the second stage of the cryo pump is shown in Figure 3.2 to reach a minimum of approximately 20 K. These pressure and temperature plots are indicative of all runs conducted for this work.

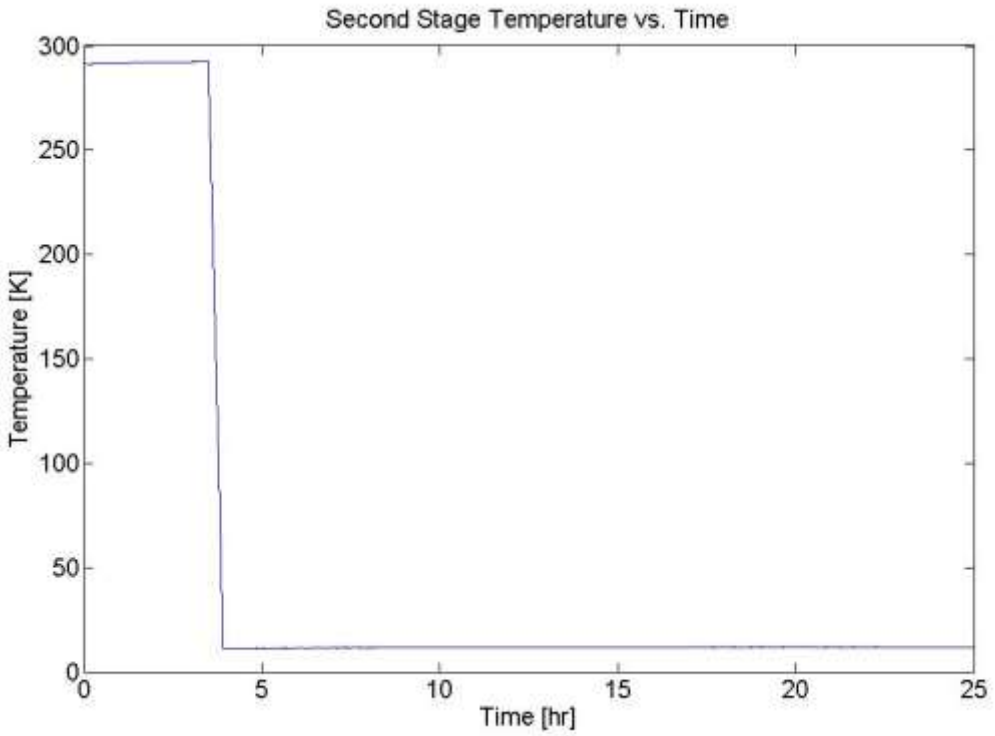

Figure 3.2: Second stage temperature during pump down process.

3.2 Elliptical Beam Interferometer

Once the main chamber pressure and temperature of the mirror reached relatively stable values, the zeolite section was opened, and water molecules were allowed to flow into the chamber. The first set of experimental runs used the interferometer setup with no expansion. This was done to check the alignment of optical components and measure ice accumulation in one location simultaneously with the QCM.

3.2.1 Ice Film Thickness Comparisons

The first experimental run was conducted under the conditions listed in Table 3.1. An effort was made to achieve temperatures around 30 K for the mirror housing and QCM housing. However even with the shield on, the radiation from the chamber walls kept the temperatures of both above 30 K. The temperature difference between the mirror housing and QCM housing measured by the

cryogenic linear temperature sensors was due to the thermal contact with the aluminum bracket. Due to the design of the housings, the QCM had a thermal contact area of 5.832 cm^2, and the mirror mount housing had a thermal contact area of 2.26 cm^2. This allowed for greater conduction of heat from the QCM than the mirror.

Table 3.1: Conditions for run #1.

Main chamber pressure	$9x10^{-9}$ torr
Mirror housing temperature	59 K
QCM housing temperature	45 K
Duration of run	43 hours

Figure 3.3 shows the ice film measurements made during run #1. The solid curve is the thickness in microns measured by the mass deposited on the QCM. The curve with symbols is the thickness in microns measured by the optical interference setup. The ratio of interference beam intensity over reference beam intensity from the interferometer for the first 8 hours is shown in Figure 3.4. The data was placed into a reduction program given by Smith [19] and resulted in the optical thickness as a function of time shown in Figure 3.3.

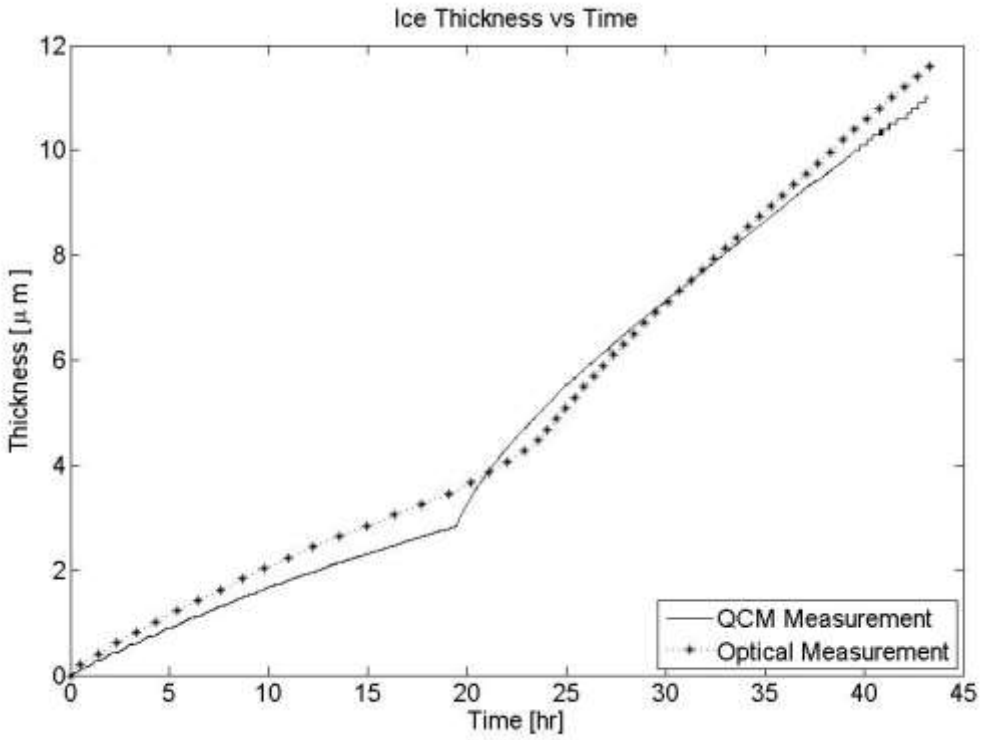

Figure 3.3: Ice film thickness from run #1.

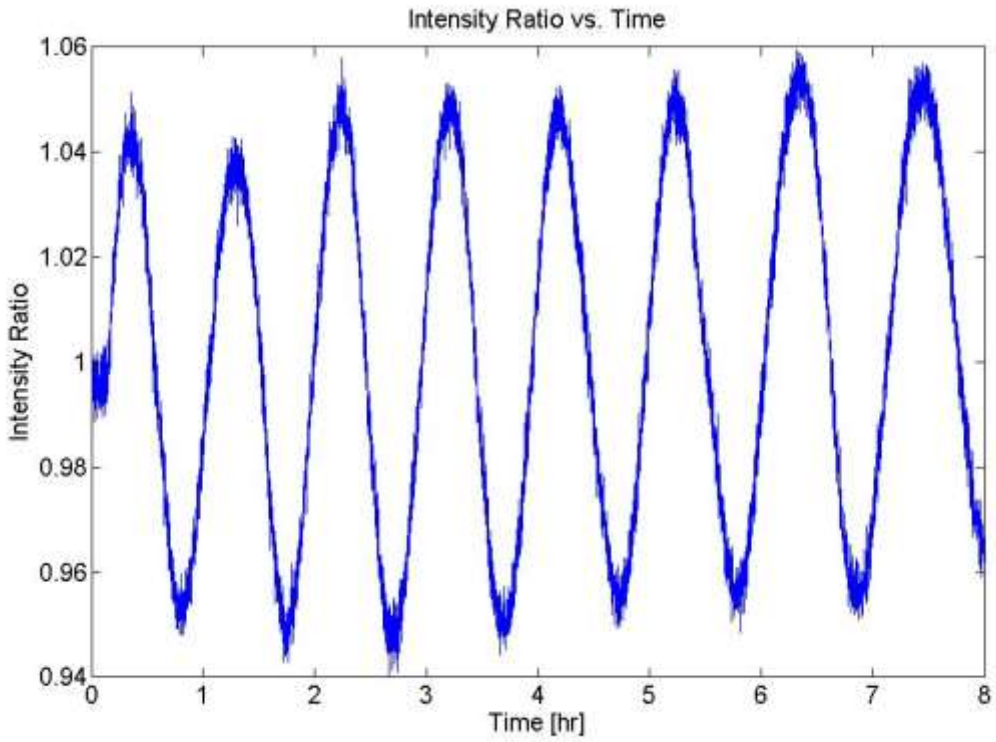

Figure 3.4: Intensity ratio from run #1.

In Figure 3.3 the sharp increase in the ice thickness around 20 hours was caused by the zeolite introduction valve being opened further at that time, which allowed a faster flow rate of water molecules. It is also noted that there is a slight delay between the optical and QCM measurements which is a result of the time averaging of the optical data over each period of modulation occurring in the data reduction program. The periodic behavior in Figure 3.4 is indicative of the phase shift occurring due to the light traveling through the ice film as discussed in Section 1.2.6. Also, the data acquisition system started recording about 20 minutes before the zeolite section valve was opened. This explains the constant intensity ratio at the beginning of Figure 3.4.

The second experimental run was conducted under the conditions listed in Table 3.2.

Table 3.2: Conditions for run #2.

Main chamber pressure	6.6×10^{-9} torr
Mirror housing temperature	57.8 K
QCM housing temperature	45 K
Duration of run	8.5 hours

Experimental run #2 was the final run using the unexpanded beam interferometer. The conditions were nearly identical to run #1 except for a lower chamber pressure. Figure 3.5 shows the ice thickness results from run #2.

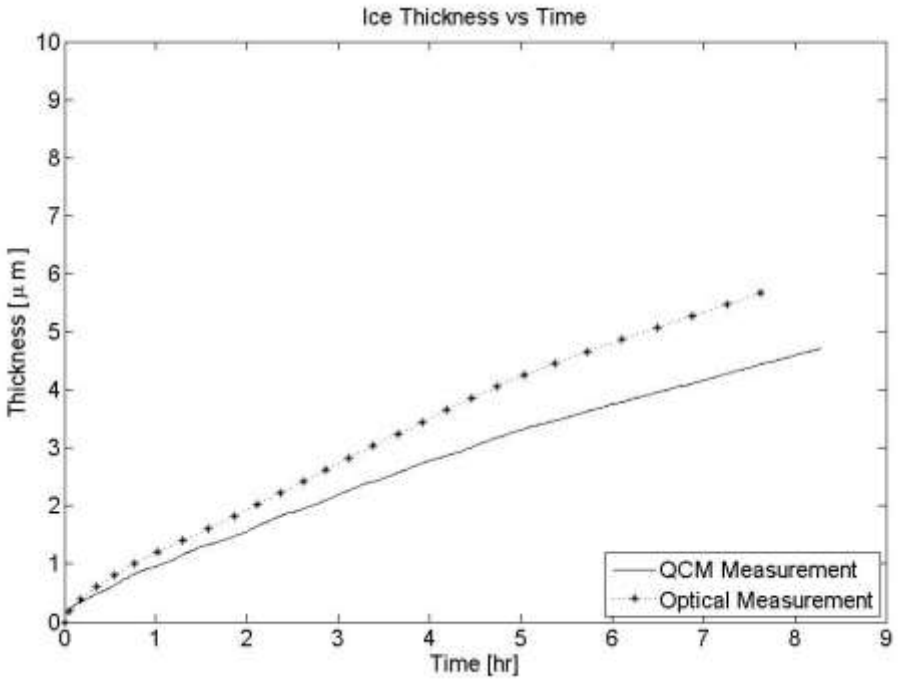

Figure 3.5: Ice film thickness from run #2.

One important comment to make about Figure 3.5 is the final ice thickness measurements made by the interferometer and QCM differ by about 21%. The QCM used for this experiment was not brand new and had been used previously. The crystal in the QCM may have gone bad after repeated use and resulted in the error. Therefore, after run #2 the crystal in the QCM was replaced with a new one to help decrease the measurement error. Another important comment is that the optical measurement stops about 1 hour before the QCM measurement. This is likely due to the ice film fracturing at 7.5 hours. Once the ice film fractured, the intensity ratio was no longer a clean signal and the data reduction program could not compute a thickness. Figure 3.6 shows the intensity ratio from 5 to 8.5 hours when the ice film fractured. Figure 3.7 shows the ice film on the mirror after fracturing occurred.

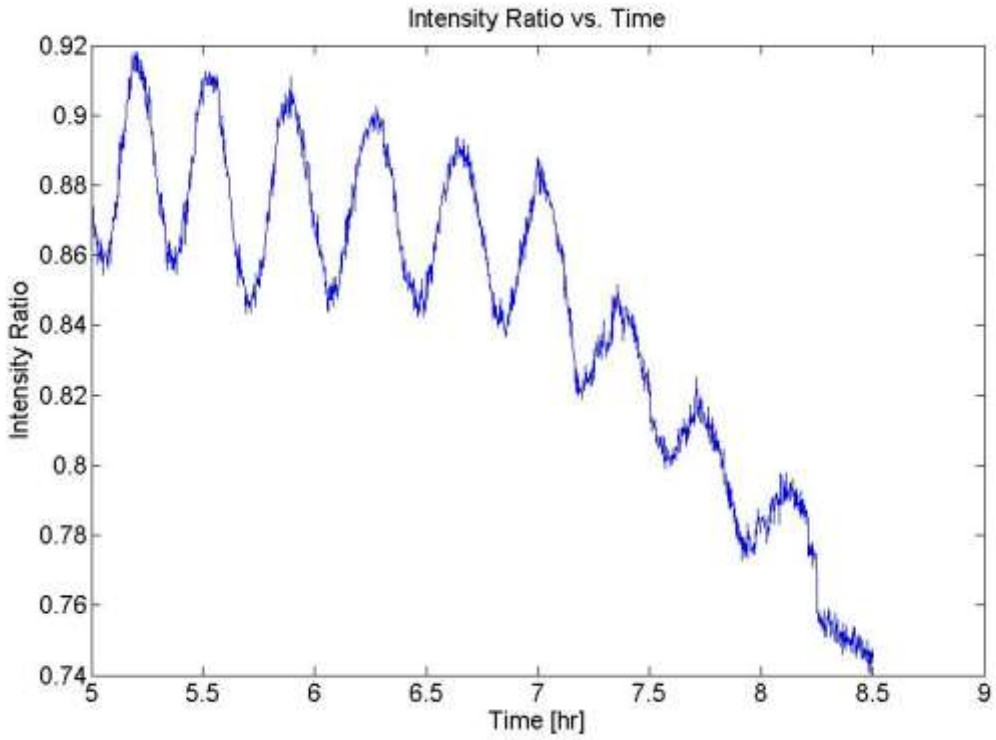

Figure 3.6: Intensity ratio from run #2.

Figure 3.7: Fractured ice film from run #2.

3.3 Expanded Elliptical Beam Interferometer

The next set of experimental runs used the expanded beam interferometer. The 4X beam expander was mounted on the laser, and a new photodiode array was fabricated to incorporate more measurement locations. Three photodiodes were used for the expanded beam instead of just one used in the unexpanded beam interferometer. Figure 3.8 shows the photodiode array used for the expanded beam experiments. Photodiode #3 (or PD3) was in the same location for the unexpanded beam experiments.

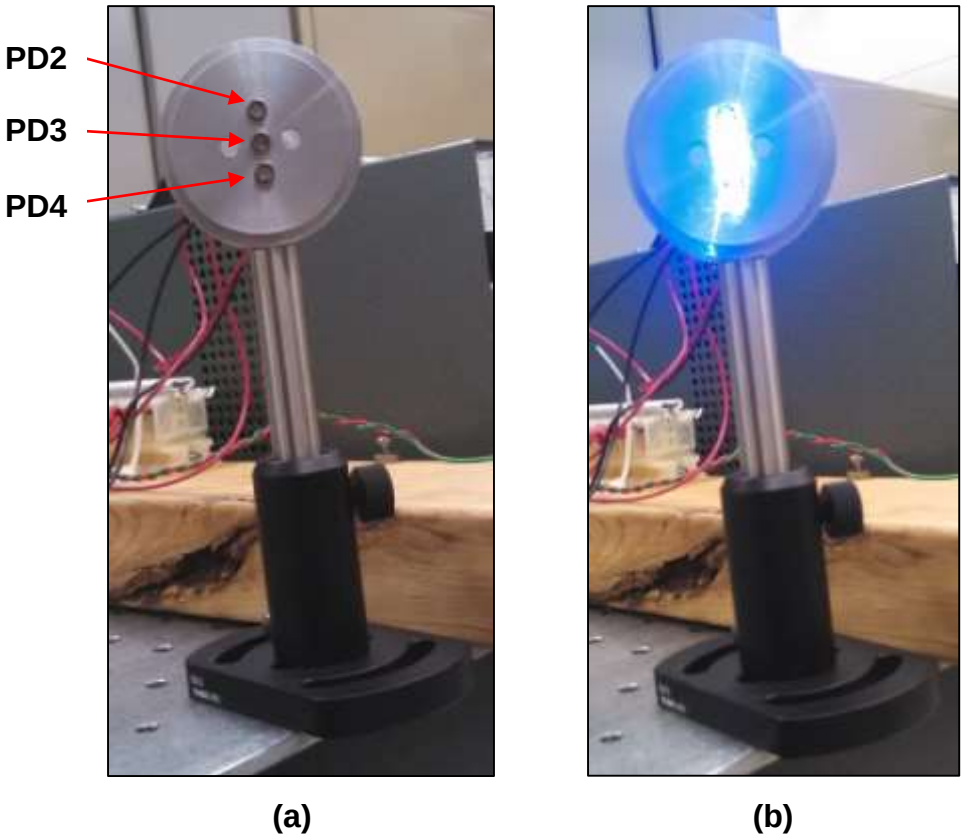

Figure 3.8: New photodiode array showing **(a)** photodiode placement and **(b)** illumination by the expanded beam.

3.3.1 Ice Film Thickness Comparisons

For this set of experimental runs the ice film thickness was computed in three different locations as shown in Figure 3.8. Run #3 was conducted under the conditions shown in Table 3.3.

Table 3.3: Conditions for run #3.

Main chamber pressure	3.2×10^{-9} torr
Mirror housing temperature	53 K
QCM housing temperature	42 K
Duration of run	13 hours

The different thickness measurements are shown in Figure 3.9.

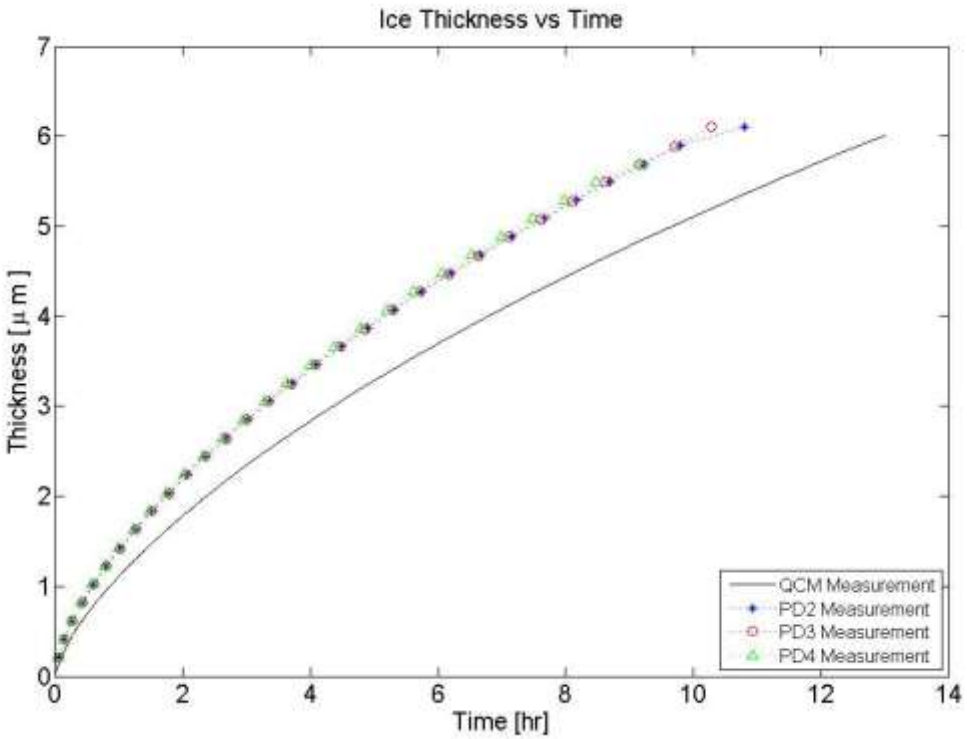

Figure 3.9: Ice film thickness from run #3.

The three colored curves (PD2, PD3, and PD4) shown in Figure 3.9 are the ice thickness measurements made by the photodiodes at locations 2, 3, and 4 (see Figure 3.8). Because the photodiodes were only separated by about 0.3 inches, the resulting thickness measurements were very similar. However, it was noticed again that the QCM measurements were significantly lower than the optical measurements. After replacing the crystal in the QCM, it was determined that the only possible explanation was that the effusion cell was not properly aligned. A misalignment of the effusion cell in the direction of the mirror caused more water molecules to be introduced on the mirror surface. Therefore after re-aligning the effusion cell, a smaller measurement error between the QCM and optical setup was expected for the next run.

Run #4 was conducted under the conditions shown in Table 3.4.

Table 3.4: Conditions for run #4.

Main chamber pressure	1.88×10^{-9} torr
Mirror housing temperature	61 K
QCM housing temperature	42 K
Duration of run	10 hours

The ice film thickness results for run #4 are shown in Figure 3.10. Once again, the three different optical measurements were very similar. However, it should be noted that the QCM measurement was much closer to the optical measurements after the re-alignment of the effusion cell. Figure 3.11 shows the intensity ratios from the three photodiodes during run #4. It was not necessary for the ratios to have the same magnitude as long as a periodic behavior was recorded. These three different intensity plots were placed in the data reduction program given by Smith [19] to determine the thickness vs time curves shown in Figure 3.10.

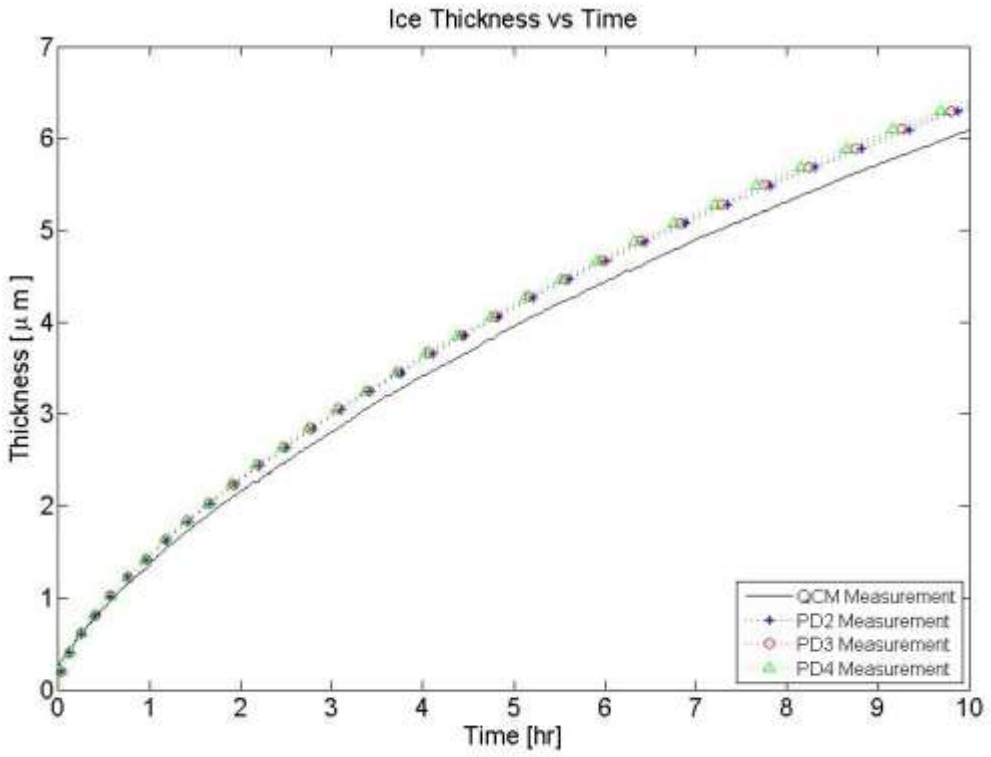

Figure 3.10: Ice film thickness from run #4.

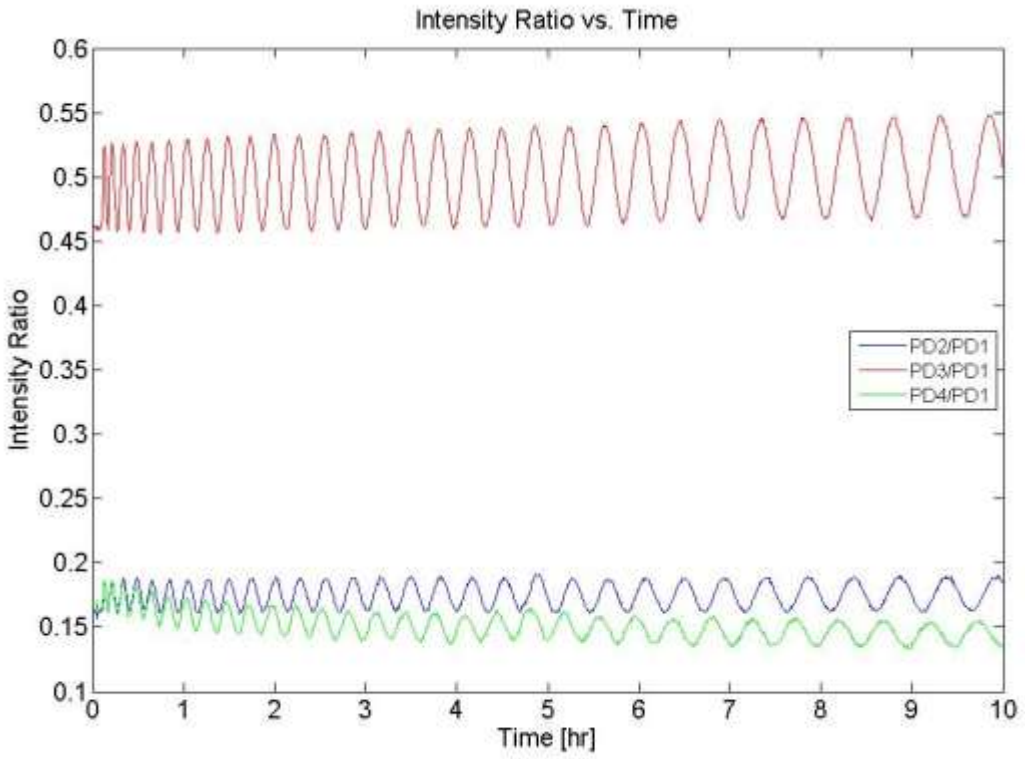

Figure 3.11: Intensity ratio from run #4.

The final run to be shown produced the closest agreement between optical and QCM thickness measurements from any of the runs. The effusion cell had been properly aligned, and the ice film did not fracture during the run. Therefore, run #5 measured ice film thickness values for up to almost 14 hours with approximately a 2.8% difference in final optical and QCM results. Table 3.5 shows the conditions for run #5, and Figure 3.12 shows the results from run #5.

Table 3.5: Conditions for Run #5.

Main chamber pressure	1.34×10^{-9} torr
Mirror housing temperature	62 K
QCM housing temperature	60 K
Duration of run	13.5 hours

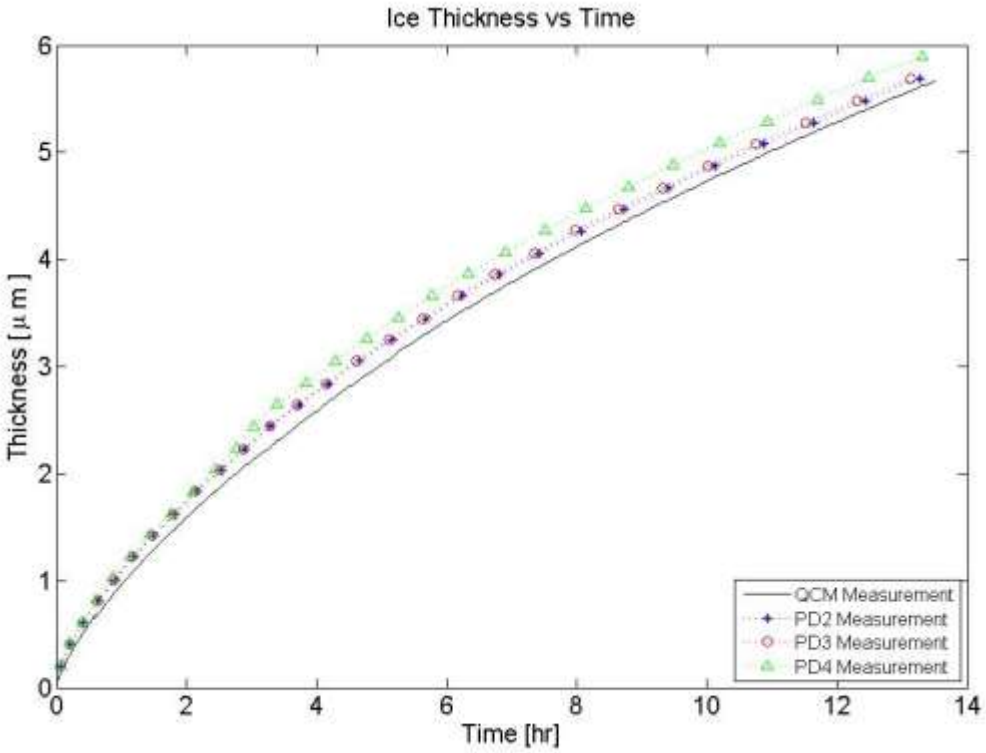

Figure 3.12: Ice film thickness from run #5.

The next table shows a comparison of all of the experimental runs including both unexpanded and expanded beam optical measurements and QCM measurements. Runs #1 and #2 correspond to the unexpanded beam measurements made with only one photodiode. Runs #3 - #6 correspond to the expanded beam ice film thickness measurements made in three different locations simultaneously. The final ice thickness measurements from the optical technique and QCM at the end of each run are shown in Table 3.6. Run #1 recorded the thickest ice film due to the long duration. The mean ice film thickness measurements from the three photodiodes of each run were compared with the corresponding QCM measurements.

The best agreement between measurements were made in run #5 with a 2.8% difference between final measurements made by the QCM and the final average thickness measurements made by the three photodiodes. Smith [19] gives a maximum uncertainty of ± 20nm for the optical interferometer monitoring technique which corresponds to roughly a 0.35% difference from QCM results. The distinction in percent difference results from the experimental runs compared to that given by Smith [19] is likely due to a slight misalignment of the effusion cell in the chamber as well as the temperature difference between the mirror and QCM surfaces. Any minor offset of the effusion cell alignment in the direction of the mirror would cause a greater distribution of water molecules to be incident on the mirror surface resulting in thicker ice film measurements.

Table 3.6: Ice thickness measurements from all experimental runs.

	Duration	**PD2**	**PD3**	**PD4**	**Mean**	**QCM**	**% diff.**
Run #1	43 hr	-	11.6 μm	-	11.6 μm	11.0μm	5.17 %
Run #2	8.5 hr	-	5.68 μm	-	5.68 μm	4.44μm	21.8 %
Run #3	13 hr	5.69 μm	5.69 μm	5.69 μm	5.69 μm	4.83μm	15.1 %
Run #4	10 hr	6.29 μm	6.30 μm	6.30 μm	6.30 μm	6.05μm	3.9 %
Run #5	13.5 hr	5.69 μm	5.69 μm	5.90 μm	5.76 μm	5.60μm	2.8 %
Run #6	7 hr	4.07 μm	4.07 μm	4.08 μm	4.07 μm	3.77μm	7.4 %

4. CONCLUSIONS AND FUTURE WORK

4.1 Conclusions

An experiment was performed to measure the accumulation of water ice on a first surface gold mirror under cryogenic, high-vacuum conditions using a 450 nm elliptical beam laser and a frequency based QCM setup. The expanded beam multiple beam interference technique was found to be a feasible method for measuring ice accumulation as a function of time at multiple locations on an optical surface. Comparisons of optical data with QCM thickness measurements taken simultaneously have shown that the expanded beam technique is as accurate as the conventional QCM thin film monitoring technique.

The optical monitoring was also found to be more reliable over thicker ice layers. As the ice accumulation increased, the slightly curved surface of the crystal occasionally caused the film to peel away from the surface resulting in QCM failure. The optical technique did not experience this problem. However, if the ice film fractured on the mirror surface, the optical data was no longer valid for use in the thickness monitoring program due to the light attenuation. Data suggests that there might be a correlation between the ice film fracturing and the temperature of the optical surface during accumulation [21]. However at this point, ice film fracture dependence on mirror surface temperature has not been thoroughly investigated and no further conclusions can be made.

The significant difference between the optical and QCM thickness measurements presented in runs #2 and #3 was attributed to the misalignment of the effusion cell. However, even with the correct alignment of the effusion cell, the optical and QCM thickness measurements still differed slightly. One possible source of error was the assumption made for the index of refraction of the water ice film, which is still uncertain for ice formed at cryogenic temperatures and low pressure. Also, due to the location of the cryogenic linear temperature sensors on the mirror mount and QCM mount, the surface temperatures of both during each experimental run was unknown. It is possible that the mirror surface was colder

than the QCM crystal collection surface during accumulation, which would result in a thicker ice film measured on the mirror.

The experiment presented is part of an on-going process to verify the capability of using multiple beam interferometry for cryodepostion measurements in high-vacuum test chambers and further developing the technology. This is a critical step in the development of an ice accumulation monitor which can be placed in critical locations within the chamber. A device such as this would greatly enhance the ability to detect ice accumulation on spacecraft optical components tested in ground test facilities and provide information as to when ice removal steps must be taken.

4.2 Future Work

In order for multiple beam interference to become a standard technique for monitoring ice accumulation on optical components in ground based testing, several areas must be further investigated. First, a better understanding of ice fracture dependency on temperature is necessary. Once the ice film fractures, the multiple beam interference technique described in this experiment fails. Therefore, if further validation is to be completed on optical monitoring, then an optimal chamber environment must be created for uninterrupted ice accumulation.

More work needs to be done to validate the conclusion that the effusion cell misalignment resulted in the error between optical and QCM thickness measurements. One way to check this conclusion would be to intentionally direct more water molecules on the QCM surface. In this case, a higher thickness measurement by the QCM would be expected. Also, horizontal measurement locations need to be utilized on the photodiode array. This would give a better idea of how the ice film thickness varies horizontally along the mirror and help validate if the effusion cell alignment is the main source of error.

Another area under current investigation is using a larger beam expander to collect data for more locations on the mirror. The results from the QCM data are predicated on the assumption that the ice film is of equal thickness over the entire surface of the crystal. However, it is shown in this experiment that the film thickness varies at different locations at a specific time. Therefore, a larger beam would allow more photodiodes to be used in the optical monitoring technique and give a better understanding of the ice accumulation on the entire surface of the mirror.

Finally, if some sort of miniature cryodeposit monitoring device is to be developed and placed at critical locations inside the chamber, then vacuum compatible components must be used. This means that the laser, optical mounts, and photo-sensors must be capable of enduring direct exposure to high-vacuum and cryogenic environments. A cryodeposit monitoring device that can be placed

at critical locations in the vacuum chamber would greatly enhance the ability to detect cryodeposit accumulation and aid in the mitigation/removal process.

BIBLIOGRAPHY

[1] Liu, C.K., “Degradation of Cold Optical Systems by Cryodeposition, Report for 1971 Independent Research Program,” *AD – 756772,* Lockheed Missiles and Space Company, Palo Alto, California, February, 1972.

[2] Westley, Michael Scott. “Vapor Deposited Water Ice: Structural Properties, Effects of Ultraviolet Light, and Astrophysical Implications.” Master’s Thesis. University of Virginia, 1994. Print.

[3] Labello, Jesse Michael. “Water Ice Films in Cryogenic Vacuum Chambers.” Ph.D. Dissertation, The University of Tennessee Space Institute, 2011. Print.

[4] M. Pashaeiyan and A. Bahari, “Nano structural properties of stainless steel for Ultra high vacuum chambers,” *International Journal of ChemTech Research*, vol.3, No. 1, pp. 403-407, 2011.

[5] D.R. Lide, Ed., *CRC Handbook of Chemistry and Physics,* 86th ed., p.6-5, CRC Press, Boca Raton, FL, 2005.

[6] Rogers, James Philip. “Introducing Water Vapor into a High Vacuum Chamber at AEDC,” Master’s Thesis. The University of Tennessee Space Institute, 2011. Print.

[7] Shah, Yatish T., “Theory of Frost Formation,” Ph.D. Dissertation, Massachusetts Institute of Technology, 1968.

[8] Trevor M. Moeller, L. Montgomery Smith, Frank G. Collins, Jesse M. Labello, James P. Rogers, Heard S. Lowry, Dustin H. Crider, “Measurement of the accumulation of water ice on optical components in cryogenic vacuum environments,” *Optical Engineering,* vol. 51(11), 115601 pp. 1-8, 2012.

[9] G. Sauerbrey, “Use of crystal oscillators for weighing thin films and for microweighing,” *Zeitschrift fuer Physik,* vol. 155(2), pp. 206-222, 1959.

[10] "Quartz Crystal Microbalance Theory and Calibration," Stanford Research Systems, www.thinksrs.com.

[11] Benes, E., "Improved quartz crystal microbalance technique," *J. Appl. Phys.* 56(3), 608 – 626, 1984.

[12] Tempelmeyer, K.E., Wood, B.E., Mills, Jr., D.W., "In Situ Measurement of Thickness and Other Properties of Carbon Dioxide Cryodeposits by Optical Techniques," *AEDC-TR-67-226*, ARO Inc., December, 1967.

[13] M.S. Westley, G. A. Baratta, and R. A. Baragiola, "Density and index of refraction of water ice films vapor deposited at low temperatures," *The Journal of Chemical Physics,* vol. 108(8), pp. 3321-3326, 1998.

[14] Eugene Hecht and Alfred Zajac. "Optics." Addison-Wesley, 1974. Print.

[15] Metz, J., "The geometry of Snell's law," *The Physics Teacher,* vol. 52, p.177, 2014.

[16] Warren, S.G., "Optical constants of ice from the ultraviolet to the micro-wave," *Appl. Opt.* 23(8), 1206 – 1225, 1984.

[17] Palik, E.D., *Handbook of Optical Constants of Solids,* Academic Press, Orlando, FL, 1985.

[18] Wood, B.E., and Smith, A.M., "Infrared Reflectance and Refractive Index of Condensed Gas Films on Cryogenic Mirrors," AIAA Paper 78-851, 2nd AIAA/ASME Thermophysics and Heat Transfer Conference, Palo Alto, California, May 1978.

[19] L. Montgomery Smith, "Cryodeposit Optical Data Processing Error Analysis," Technical Report for Physical Sciences Inc., University of Tennessee Space Institute, 2015.

[20] “CH-210 Cold Head Operating Manual,” Sumitomo Cryogenics of America Inc., Revision B, 2007.

[21] Trevor M. Moeller, L. Montgomery Smith, Frank G. Collins, Jesse M. Labello, James P. Rogers, Heard S. Lowry, Dustin H. Crider, “Further results in measuring water ice buildup on optical components in cryogenic vacuum chambers,” *SPIE Digital Library*, vol. 8841, pp. 1-12, University of Tennessee Space Institute, Arnold Engineering Development Complex, 2013.

VITA

William Hayden Stevens was born and raised in Nashville, Tennessee. He received a Bachelor's of Science degree in Mechanical Engineering from Tennessee Technological University in Cookeville, Tennessee. He went on to study at the University of Tennessee Space Institute in Tullahoma, Tennessee, where he is currently being awarded his Masters of Science degree in Mechanical Engineering. His areas of interest include space technology, combustion, and high speed flows.